CPSF3 inhibition blocks pancreatic cancer cell proliferation through disruption of core histone mRNA processing

Abdulrahman. A. Alahmari[1,2], Aditi H. Chaubey[1], Venkata S. Jonnakuti[3,4,5], Arwen A. Tisdale[1], Carla D. Schwarz[1], Abigail C. Cornwell[1], Kathryn E. Maraszek[1], Emily J. Paterson[1], Minsuh Kim[1], Swati Venkat[1], Eduardo Cortes Gomez[6], Jianmin Wang[6], Katerina V. Gurova[7], Hari Krishna Yalamanchili[3,8,9], and Michael E. Feigin[1, *]

[1]Department of Pharmacology and Therapeutics, Roswell Park Comprehensive Cancer Center, Buffalo, NY 14203

[2]Department of Medical Laboratory Sciences, College of Applied Medical Sciences, Prince Sattam Bin Abdulaziz University, Alkharj 11942, Saudi Arabia

[3]Department of Pediatrics, Baylor College of Medicine, Houston, TX 77030

[4]Program in Quantitative and Computational Biology, Baylor College of Medicine, Houston, TX 77030

[5]Medical Scientist Training Program, Baylor College of Medicine, Houston, TX 77030

[6]Department of Biostatistics and Bioinformatics, Roswell Park Comprehensive Cancer Center, Buffalo, NY 14203

[7]Department of Cell Stress Biology, Roswell Park Comprehensive Cancer Center, Buffalo, NY 14203

[8]Jan and Dan Duncan Neurological Research Institute at Texas Children's Hospital, Houston, TX 77030

[9]USDA/ARS Children's Nutrition Research Center, Department of Pediatrics, Baylor College of Medicine, Houston, TX 77030

*Corresponding author:

Email: michael.feigin@roswellpark.org

Keywords: CPSF3, JTE-607, Alternative polyadenylation, Histone processing, Chromatin stability

ABSTRACT

Pancreatic ductal adenocarcinoma (PDAC) is a lethal disease with limited effective treatment options, potentiating the importance of uncovering novel drug targets. Here, we target Cleavage and Polyadenylation Specificity Factor 3 (CPSF3), the 3' endonuclease that catalyzes mRNA cleavage during polyadenylation and histone mRNA processing. We find that *CPSF3* is highly expressed in PDAC and is associated with poor prognosis. *CPSF3* knockdown blocks PDAC cell proliferation and colony formation *in vitro* and tumor growth *in vivo*. Chemical inhibition of CPSF3 by the small molecule JTE-607 also attenuates PDAC cell proliferation and colony formation, while it has no effect on cell proliferation of non-transformed immortalized control pancreatic cells. Mechanistically, JTE-607 induces transcriptional read-through in replication-dependent histones, reduces core histone expression, destabilizes chromatin structure and arrests cells in the S-phase of the cell cycle. Therefore, CPSF3 represents a potential therapeutic target for the treatment of PDAC.

INTRODUCTION

Pancreatic ductal adenocarcinoma (PDAC) is the third leading cause of cancer-related deaths with a five-year survival rate of 12%, due in part to the lack of effective treatment options (Siegel et al. 2023). PDAC is primarily driven by mutations in the oncogene *KRAS* and several tumor suppressors, including *TP53*, *CDKN2A* and *SMAD4* (Kleeff et al. 2016). However, as clinically effective modulators of activity of these proteins are not currently available, identification of novel targets amenable to small molecule inhibition is a critical undertaking. Recently, large-scale RNA sequencing efforts of PDAC tumors have revealed widespread dysregulation of oncogenic gene expression, allowing the characterization of several PDAC subtypes and phenotypic states (Collisson et al. 2011; Moffitt et al. 2015; Bailey et al. 2016; Peng et al. 2019). These gene expression changes are critical for driving tumor phenotypes, including metastatic progression (Wang et al. 2019; Abel et al. 2018; Roe et al. 2017; Sodir et al. 2020; Shankar et al. 2016). While these gene expression changes have been extensively catalogued, the mechanisms underlying this transcriptional heterogeneity remain largely unknown (Venkat et al. 2021). We propose that targeting these drivers of dysregulated gene expression represents an opportunity to reverse widespread oncogenic activity in transformed cells.

One such gene regulatory process that has been implicated in cancer is mRNAs processing, a step that is crucial for maturity of newly transcribed RNAs. For most human genes, nascent RNAs undergo cleavage and polyadenylation, or CPA. Because most genes have multiple polyadenylation recognition sites (PASs) within the 3' untranslated region (UTR), the choice of where mRNA is cleaved and polyadenylated can generate distinct transcript isoforms with different 3'UTR lengths, ultimately affecting mRNA stability, localization and translation (Gruber and Zavolan 2019). This process is called alternative polyadenylation, or APA, and is widely dysregulated in cancer (Gruber and Zavolan 2019; Yuan et al. 2019; Masamha and Wagner 2018). Recently, we identified widespread APA alterations in PDAC patients that are associated with functional changes in both gene and protein expression of growth-promoting genes (Venkat et al. 2020). Unlike polyadenylated genes, a class of histone genes are processed on the mRNA level by cleavage but not polyadenylation. These histones are replication-dependent and are crucial for cell proliferation. While CPA and histone mRNA processing are regulated by two different complexes, some proteins are in fact important regulators of both processes. One such protein that is the focus of our study is Cleavage and Polyadenylation Specificity Factor 3 (CPSF3) (Sullivan et al. 2009b), the endonuclease responsible for the cleavage of mRNAs. As a part of the

CPA complex, CPSF3 cooperates with other CPA factors to cleave the mRNA prior to the addition of the poly(A) tail. As part of the histone cleavage complex (HCC), however, CPSF3 cleaves pre-mRNAs of replication-dependent core histones, but these pre-mRNAs do not get polyadenylated. Both CPA and histone mRNA processing are important biological processes for cell proliferation and survival. The fact that CPSF3 is an enzyme opens the possibility of its pharmacological targeting. Recently, CPSF3 was identified as the target of the small molecule JTE-607 (Kakegawa et al. 2019; Ross et al. 2020). JTE-607 is hydrolyzed into an active compound that directly interacts with the CPSF3 interfacial cavity (Ross et al. 2020). This interaction inhibits CPSF3 catalytic activity leading to accumulation of unprocessed newly synthesized pre-mRNAs. JTE-607 induces apoptosis of human acute myeloid leukemia (AML) and Ewing's sarcoma cells *in vitro* and prolongs survival of tumor-bearing mice in xenograft models *in vivo* (Uesato et al. 2006; Tajima et al. 2010). JTE-607 inhibits migration, invasion and self-renewal of breast cancer cells (Liu et al. 2022). Notably, administration of JTE-607 in healthy volunteers demonstrated the safety of this compound in humans, with no severe adverse events reported (Borozdenkova et al. 2011). However, the role of CPSF3 and the effect of JTE-607 in epithelial cancers remains largely unknown.

Here, we show that knockdown and/or inhibition of CPSF3 attenuates PDAC cell proliferation *in vitro* and *in vivo*. We find that CPSF3 is highly expressed in PDAC patients and is a predictor of poor outcome. We demonstrate that small molecule inhibition of CPSF3 by JTE-607 selectively attenuates proliferation of PDAC cells but not immortalized control cells. Additionally, we conduct a global analysis of CPSF3 disruption in PDAC, uncovering gene regulatory mechanisms that distinctly affect PDAC cells upon either *CPSF3* knockdown or inhibition. We uncover that JTE-607 dysregulates replication-dependent histones, destabilizes chromatin structure and arrests cells in S-phase of the cell cycle. Overall, our findings uncover new functions of CPSF3 in cancer and nominate CPSF3 as a novel therapeutic target in PDAC.

RESULTS

CPSF3 is upregulated in human PDAC and required for PDAC cell proliferation.

To determine the clinical significance of *CPSF3* expression in PDAC, we first analyzed gene expression data from the Clinical Proteomic Tumor Analysis Consortium (CPTAC) (Cao et al. 2021). *CPSF3* expression was significantly higher in PDAC tumors (n=135), as compared with non-tumor adjacent tissues (n=18) and normal pancreata (n=7) (Fig. 1A). Consistent with this finding, *CPSF3* expression was also significantly higher in the Pancreatic Adenocarcinoma (PAAD) dataset from The Cancer Genome Atlas (TCGA) (n=147) as compared to normal pancreata (n=165) from The Genotype-Tissue Expression (GTEx) project (Fig. 1B). We then sought to assess *CPSF3* expression status in our cell line models. In agreement with the clinical data, we found that *CPSF3* is upregulated in PDAC cell lines (MiaPaCa2, Suit2, Panc1) as compared to non-transformed immortalized pancreatic epithelial cells (HPNE and HPDE; from now on referred to as immortalized control cells) by western blot (WB) and RT-qPCR (Fig. 1C and Fig. S1A). Other CPA factors were also upregulated in our PDAC cell lines compared to immortalized control HPNE cells (Fig. S1B – S1I). This is consistent with our previous report where multiple CPA factors are upregulated in PDAC patients (Venkat et al. 2020). We chose to focus on CPSF3 as it is an enzyme and therefore is a potential druggable target. We then sought to assess the relationship between *CPSF3* expression and PDAC patient outcome. Patients with high *CPSF3* expression had significantly worse overall survival than patients with low *CPSF3* expression (P=0.00164, hazard ratio 5.047 (1.842-13.827)). Specifically, patients in the top quartile of *CPSF3* expression had a median survival of 14.2 months, while those in the bottom quartile of *CPSF3* expression had a median survival of 33.5 months (Fig. 1D). Therefore, *CPSF3* is highly expressed in PDAC, high expression correlates with poor patient outcome, and our cell models are appropriate for mechanistic studies.

To define the functional role of *CPSF3* in PDAC we first took a genetic approach and generated stable *CPSF3* knockdown MiaPaCa2 and Panc1 cells. We used two different short hairpin RNAs (sh1 and sh2) targeting *CPSF3*, and a non-targeting control (shNTC). Successful knockdown of *CPSF3* was confirmed at the protein and RNA level by WB and RT-qPCR, respectively, with sh1 cells having the highest level of knockdown in both cell lines (Fig. 1E and Fig. S2A). We then examined the effect of *CPSF3* knockdown on cell proliferation and colony formation capability. *CPSF3* knockdown significantly attenuated proliferation as compared with shNTC controls in both MiaPaCa2 and Panc1 cells (Fig. 1F). *CPSF3* knockdown also significantly decreased colony formation (Fig. S2B and S2C). In both the proliferation and colony formation assays, and in both

PDAC cell lines, sh1 CPSF3 had the strongest phenotype, consistent with higher levels of *CPSF3* knockdown. In contrast, knockdown of *CPSF3* in immortalized HPNE cells had no effect on proliferation (Fig. S2D and S2E). Next, we sought to determine the requirement for CPSF3 in PDAC tumor growth *in vivo*. We implanted MiaPaCa2 cells (either shNTC or sh1 CPSF3, $5x10^5$ per mouse) subcutaneously into the flanks of NOD/SCID/IL2Rγ$^{-/-}$ (NSG) mice. *CPSF3* knockdown tumors grew significantly slower, and weighed significantly less at endpoint, than shNTC tumors (Fig. 1G, Fig. S3A and S3B). No changes in tumor histopathology were noted by Hematoxylin and Eosin (H&E) staining (Fig. S3C). Immunohistochemical (IHC) analysis revealed that CPSF3 knockdown was maintained *in vivo* (Fig. S3D). Finally, IHC for Ki67 revealed a significant decrease in proliferation in *CPSF3* knockdown tumors as compared with shNTC controls (Fig. S3E). Overall, these data support the requirement for CPSF3 in PDAC cell proliferation and tumor growth.

PDAC cells are sensitive to chemical inhibition of CPSF3.

CPSF3 was recently identified as the target for the small molecule JTE-607. JTE-607 is a prodrug that, when metabolized by the ester hydrolyzing enzyme carboxylesterase 1 (CES1), binds to CPSF3 and inhibits its catalytic activity, impairing the processing of newly synthesized mRNAs (Ross et al. 2020). As genetic depletion of *CPSF3* attenuated PDAC cell proliferation (Fig. 1), we hypothesized that pharmacologic inhibition of CPSF3 with JTE-607 could represent a novel therapeutic approach in PDAC. We therefore examined the sensitivity of multiple human pancreatic cell lines, both immortalized control cells and PDAC, to JTE-607 in a 72-hour dose-response cell viability assay. Immortalized control pancreatic epithelial cells (HPNE, IC50=130.4μM; HPDE, IC50=60.11μM) and human cancer associated fibroblast cell lines (C7 CAF, IC50=70.04μM; PancPat CAFs, IC50=114.2 μM) were not sensitive to JTE-607 (Fig. 2A and 2B). In contrast, human PDAC cell lines displayed a range of sensitivities to JTE-607, with Panc1 cells being the most sensitive (IC50=2.163μM) (Fig. 2A). Importantly, the relationship between cell line doubling time and JTE-607 sensitivity shows that sensitivity to JTE-607 was associated with proliferation rate (Fig. 2C). Next, we determined the effect of JTE-607 on cell proliferation by treating cells with increasing concentrations of JTE-607 and assessing cell viability in a time-dependent fashion (Fig. 2D and 2E). JTE-607 had no effect on proliferation in HPNE cells (Fig. 2D). However, proliferation of MiaPaCa2 and Panc1 PDAC cells was significantly attenuated by JTE-607, in a dose-dependent manner (Fig. 2E). Finally, we tested the effect of JTE-607 on colony formation in PDAC cell lines. JTE-607 significantly decreased colony formation in all PDAC

cell lines tested (Fig. 2F and Fig. S4A- S4D). Therefore, JTE-607 selectively attenuates proliferation of PDAC cells over immortalized control pancreatic cells.

mRNA 3'-end processing is distinct between knockdown and chemical inhibition of CPSF3. Because JTE-607 inhibits CPSF3 catalytic activity without inducing target degradation, we sought to understand if the function of CPSF3 is distinct between knockdown and inhibition. As CPSF3 is an integral component of the cleavage and polyadenylation (CPA) complex and the histone cleavage complex (HCC) (Sullivan et al. 2009b; Wagner et al. 2007; Yang et al. 2020), we hypothesized that CPSF3 disruption would affect both alternative polyadenylation (APA) and histone mRNA processing. To test this hypothesis, we subjected *CPSF3* knockdown and JTE-607-treated Panc1 cells to RNA-sequencing (Whole transcriptome sequencing with ribosomal RNA depletion and primed with random priming). Next, we performed APA analysis using polyAMiner-Bulk to uncover significantly altered changes in 3'-UTR length (Jonnakuti et al. 2023; Yalamanchili et al. 2020). Briefly, polyAMiner-Bulk detects alternative polyadenylation alterations from bulk RNA-seq data (see Materials and Methods for details) by generating a poly A index score (PolyAIndex) for each gene based on the relative abundances of 3′-UTR long and short forms. Cleavage at a proximal polyadenylation signal (pPAS) generates a short 3'-UTR, while cleavage at a distal polyadenylation signal (dPAS) generates a long 3'-UTR. A negative PolyAIndex indicates a shortening event, and a positive PolyAIndex indicates 3'-UTR lengthening. To identify differential APA genes (DAGs) with minimum false positives/negatives and better understand the differences between knockdown and inhibition, we chose a stringent PolyAIndex threshold (-0.5> PolyAIndex >0.5; Padj < 0.05) (Table S1). In the *CPSF3* knockdown cells, PolyAMiner-Bulk detected 85 significant DAGs, of which 43 genes underwent 3'UTR lengthening (PolyAIndex > 0.5; Padj < 0.05) and 42 genes underwent 3'UTR shortening (PolyAIndex < -0.5; Padj < 0.05) (Fig. S5A). In the CPSF3 inhibition model, PolyAMiner-Bulk detected 174 significant DAGs, of which 138 underwent 3'UTR lengthening (PolyAIndex > 0.5; Padj < 0.05) and 36 genes underwent 3'UTR shortening (PolyAIndex < -0.5; Padj < 0.05) (Fig. S5B). Of note, JTE-607 treatment exhibited more DAGs than *CPSF3* knockdown, with genes undergoing lengthening events being the most predominant. Surprisingly, however, the DAGs identified in both *CPSF3* knockdown and inhibition do not converge, with only two shared DAGs altered in the same-direction between both conditions (Fig. S5C).

To determine if these distinct patterns are due to differences in CPA complex stability upon *CPSF3* knockdown or inhibition, we performed immunoprecipitation (IP) experiments to pull-down multiple CPA complexes. The CPA machinery is composed of multiple complexes including the

cleavage and polyadenylation specificity factor (CPSF) complex, the cleavage stimulation factor (CSTF) complex, and the cleavage factor (CFI and CFII) complexes. The CPSF complex forms two subcomplexes, the mammalian polyadenylation specificity factor (mPSF) containing CPSF1, WDR33, FIP1 and CPSF4 which recognizes the AAUAAA PAS, and the mammalian cleavage factor (mCF) subcomplex containing CPSF2, CPSF3 and Symplekin which possesses endonucleolytic activity (Shi and Manley 2015). We found that *CPSF3* knockdown, but not inhibition, destabilizes the CPA complex (Fig. S6A – S6C). The amount of CPSF2 and CPSF3 bound to CPSF4 decreases upon *CPSF3* knockdown, consistent with their heterodimer function (Fig. S6A). The other CPA factors probed show increased basal protein levels upon *CPSF3* knockdown (Fig. S6A, input columns). Protein levels of CSTF2 and NUDT21, which bind to U/GU-rich elements downstream of PAS and UGUA-rich element upstream of PAS, respectively, both increase upon *CPSF3* knockdown. Therefore, stability of the CPA complex upon *CPSF3* knockdown may at least partially be attributed to dysregulated basal protein levels of multiple CPA factors. On the other hand, CPSF3 inhibition did not affect the stability or basal protein levels of CPA complexes (Fig. S6B). Of note, knockdown or inhibition of CPSF3 did not largely affect CPA factor expression on the mRNA level (Fig. S6D and S6E), indicating that the effect of *CPSF3* knockdown on CPA factor expression is not transcriptional.

To better understand the difference between knockdown and inhibition, we next asked which type of *cis*-elements are regulated in both conditions, thus influencing PAS selection. Multiple *cis*-elements have been shown to promote APA in an opposing manner. For example, the CPA factor FIP1 binds to an A-rich sequence upstream of the canonical AAUAAA PAS (upstream sequence element, or USE) and promotes the usage of proximal PASs, thus inducing shortening of genes (Lackford et al. 2014). In contrast, NUDT21, the small subunit of cleavage factor 1, binds to UGUA-containing USE. When binding to UGUA-containing USE near distal PASs, NUDT21 prevents the CPSF subunits from interacting with proximal PASs, thus inducing lengthening of genes (Brown and Gilmartin 2003; Martin et al. 2012). To address the 3'-end processing differences between knockdown and inhibition, we performed two independent motif enrichment analyses. First, we examined the distribution of the UGUA motif within the 3'UTR of genes that underwent shortening in both conditions. We found significant enrichment for UGUA motifs near distal PASs (~25-50 bp upstream) compared to the proximal PASs within the 3'UTR of genes that exhibit shortening changes following *CPSF3* knockdown (Fig. S7A, pink highlight). These results indicate that CPSF3 strongly binds at distal PASs of the unique 3'UTR shortened genes and that *CPSF3* knockdown shifts this PAS selection to a proximal PAS. On the other hand, CPSF3 inhibition by JTE-607 did not show consistent distribution patterns of the UGUA motif (Fig. S7B)

suggesting that enzymatic inhibition of CPSF3 may rely on other *cis*-elements to direct PAS selection. To identify which *cis*-elements are enriched upon both *CPSF3* knockdown and inhibition in an unbiased manner, we selected the genes that are uniquely identified as undergoing 3'UTR lengthening or shortening in both experiments and performed motif enrichment analysis within the 100bp upstream and downstream (50bp in each direction) of the most proximal and most distal PASs (refer to Materials and Methods in the Supplemental file for more details). We found distinct motif enrichment across *CPSF3* knockdown and inhibition at both proximal and distal PASs (Fig. S7C and S7D). For example, genes undergoing shortening upon *CPSF3* knockdown were enriched for the canonical PAS AATAAA within the pPAS (Fig. S7C, pink highlight). In contrast, a similar AATAAA sequence was enriched within the pPAS of lengthened genes upon JTE-607 treatment (Fig. S7D, blue highlight). The fact that *CPSF3* knockdown and inhibition DAGs show the consensus AATAAA signal in distinct sets (lengthened and shortened, respectively) suggest diverse polyadenylation site selection. This is also substantiated by the poor overlap of *CPSF3* knockdown and inhibition DAGs shown in Fig. S5C. Therefore, this difference suggests selection for different PASs, thus supporting the notion that *CPSF3* knockdown and inhibition differentially affect the site of polyadenylation.

JTE-607 inhibits expression of replication-dependent histones.

We next sought to understand the mechanism by which CPSF3 disruption attenuates PDAC cell proliferation. Recently, we reported widespread APA shortening events in PDAC patients that are associated with oncogenic functions (Venkat et al. 2020). Therefore, we asked whether CPSF3 disruption would reverse the APA patterns of those growth-promoting genes. However, neither *CPSF3* knockdown nor inhibition altered the APA patterns of these genes (Fig. S8A). In fact, few genes were altered on both the APA and gene expression levels by either *CPSF3* knockdown or inhibition (Fig. S8B). These data suggest that PDAC phenotype is mediated by other mechanisms in our cell line models. In addition to CPA, CPSF3 controls histone mRNA processing as part of the HCC. Therefore, we sought to understand whether CPSF3 disruption affects histone processing in PDAC cells. We performed differential gene expression analysis and were intrigued to find that numerous histone genes were significantly downregulated upon JTE-607 treatment (Fig. 3A, Blue-labeled genes). Gene set enrichment analysis (GSEA) also demonstrated a dysregulation in many histone-related pathways, including histone methylation, acetylation and deacetylation (Fig. S9A). However, *CPSF3* knockdown did not affect histone gene expression in our cell line model (Fig. S9B). In fact, the discrepancies between *CPSF3* knockdown and inhibition

extend to the overall differential gene expression with only 119 genes being differentially expressed in both conditions (Fig. S9C).

Histone genes are classified into two classes: replication-independent (RI) and replication-dependent (RD) histones. RI histones are processed on their mRNA 3'end by CPA and therefore polyadenylated. In contrast, RD histone mRNAs are processed by the HCC and are not polyadenylated (Marzluff et al. 2008). RD histones are actively transcribed during DNA replication and important for the proliferation of dividing cells. The majority of the differentially expressed histones upon CPSF3 inhibition with JTE-607 were RD histones. In contrast, RI histones were not downregulated by JTE-607 (Fig. 3B). To validate the JTE-607-induced decrease in RD histones in another PDAC cell line, we assessed mRNA levels of two RD histones (*HIST1H2BC* and *HIST1H3B*) in MiaPaCa2 cells using RT-qPCR. Similar to Panc1 cells, JTE-607 reduced RD histone mRNA levels in MiaPaCa2 (Fig. 3C). Therefore, JTE-607 treatment decreases the expression of RD histones. Finally, we sought to determine if RD histone expression predicts patient outcomes. We generated a signature by selecting 50 RD histones and assessed PDAC patient survival based on gene expression. We found that high levels of RD histones are associated with worse disease-progression ($p=0.031$, Hazard Ratio = 1.6) and poor overall survival ($p=0.0072$, Hazard Ratio = 1.8) in PDAC patients (Fig. 3D and 3E). Collectively, these results indicate that JTE-607 preferentially downregulates RD histones.

JTE-607 induces RD-histone read-through preferentially in PDAC cells.

Disruption of the HCC has been shown to induce transcriptional read-through of histone transcripts (Romeo et al. 2014; Wagner et al. 2007). While several studies have demonstrated a role for CPSF3 in histone processing (Sullivan et al. 2009b; Wagner et al. 2007; Yang et al. 2013, 2020), the effect of chemical inhibition of CPSF3 activity on histone mRNA processing has never been biologically determined. We therefore sought to investigate whether CPSF3 inhibition induces transcriptional read-through experimentally by RT-qPCR. We picked two RD- and two RI-histones that show differences beyond their 3'end boundaries for experimental validation (Fig. S10A and S10B). We then designed PCR primers to amplify different regions within and beyond the boundaries of the 3'-UTR (Fig. S10C). We found that 24h JTE-607 treatment significantly induced transcriptional read-through (up to ~20-fold change) of RD histones in Panc1 cells (Fig. 4A). However, the effect of JTE-607 on transcriptional read-through in HPNE cells was minimal (Fig. 4A). In fact, 2-hours of JTE-607 treatment were enough to induce transcriptional read-through levels in Panc1 cells comparable to those in HPNE cells after 24-hours of treatment (Fig. 4A and 4B). Importantly, JTE-607 did not induce transcriptional read-through of RI histones at

early or late time points in both Panc1 and HPNE cells (Fig. 4C and 4D). We then validated the transcriptional read-through in another cell line model, MiaPaCa2, in a dose dependent manner (Fig. S10D and S10E). We show that JTE-607 induces significant levels of read-through in RD histones as compared to RI histones. As *CPSF3* knockdown did not affect histone mRNA levels, we aimed to further delineate the differences between knockdown and inhibition in inducing transcriptional read-through. We found that long term knockdown of *CPSF3* by shRNA did not induce transcriptional read-through in both RD and RI histones (Fig. S10F). Because stable long-term knockdown can force cells to adapt, we asked whether short-term knockdown of *CPSF3* can recapitulate the JTE-607 effect on transcriptional read-through. We transiently silenced *CPSF3* using siRNA (Fig. S10G) and found that *CPSF3* silencing did not induce transcriptional read-through in both RD and RI histones (Fig. S10H). Improperly processed histone mRNAs fail to be exported into the cytoplasm for translation, leading to decreased protein levels (Sullivan et al. 2009b; Romeo et al. 2014; Sullivan et al. 2009a). Therefore, we examined RD histone protein levels upon JTE-607 treatment and found that JTE-607 reduced both H3 and H2B protein levels in a dose- and time-dependent fashion in Panc1 but not HPNE cells (Fig. S10I and S10J). Next, we determined whether histone dysregulation might be transcriptionally mediated by dysregulation of transcription factors at the levels of APA or gene expression. We used MotifMap, an integrative genome-wide map of regulatory motif sites, to find putative transcription factors regulating expression of RD histones (Daily et al. 2011). We found 51 transcription factors that have strong binding sites (1000bp upstream of transcription start site; FDR < 0.05) within RD histone promoters (Table S2). However, these histone transcription factors are neither APA altered nor differentially expressed upon JTE-607 treatment (Fig. S10K and S10L). Taken together, these findings indicate that JTE-607 decreases RD histone expression by promoting transcriptional read-through.

JTE-607 destabilizes chromatin and blocks cell cycle progression.

As replication-dependent histones are required for nucleosome assembly (Gunjan et al. 2005; Groth et al. 2007; Günesdogan et al. 2014; Marzluff et al. 2008), we hypothesized that JTE-607 would dysregulate chromatin dynamics. Gene ontology analysis of downregulated genes upon JTE-607 treatment showed an enrichment for chromatin-related processes including chromatin assembly, nucleosome assembly and nucleosome organization (Fig. S11A). Therefore, we performed a Micrococcal Nuclease (MNase) assay to assess relative chromatin condensation. Using chromatin DNA, MNase digests open DNA regions that are not stably bound by proteins, thus producing nucleosome fragmentation patterns that are indicators of whether chromatin is in

a condensed or relaxed state. The chromatin destabilizing agent CBL0137 was used as a positive control (Xiao et al. 2021). Panc1 cells treated with JTE-607 or CBL037 displayed rapid and complete chromatin digestion, as compared with DMSO-treated cells (Fig. 5A). After 30 minutes of incubation, MNase digestion released more mononucleosomes in JTE-607 (~$4x10^3$ normalized FU) as compared to DMSO (~$1.2x10^3$ normalized FU) (Fig. S11B – S11E). Because HPNE cells are insensitive to JTE-607 (Fig. 2A and 2D), we sought to determine the impact of CPSF3 inhibition on chromatin structure in HPNE cells. In contrast to Panc1 cells, HPNE cells treated with JTE-607 or CBL037 showed no chromatin digestion as compared with DMSO-treated cells (Fig. 5B). In fact, the amount of digested mononucleosomes in HPNE cells with all treatments is comparable to DMSO-treated Panc1 cells (Fig. S11F – S11I). These results suggest that JTE-607 preferentially targets cells that are in high demand for histone supplies. To assess chromatin destabilization in a living cell, we utilized the HeLa-TI cell line model that has a silenced GFP reporter within a heterochromatic region of the genome. Treatment of these cells with chromatin destabilizing agents, including CBL0137, allows derepression of GFP silencing. Therefore, we monitored GFP expression in HeLa-TI cells upon JTE-607 treatment by both florescence microscopy and flow cytometry. Cells treated with JTE-607 induced GFP expression to levels comparable with CBL0137 in a dose- and time-dependent manner (Fig. 5C-5E).

Finally, we sought to determine how JTE-607 led to defects in cell viability. As RD histones are required for cell cycle progression, we assessed the effects of JTE-607 on cell cycle distribution. In immortalized control HPNE cells, JTE-607 had no impact on cell cycle distribution (Fig. 6A and 6B). In contrast, JTE-607 arrested Panc1 and MiaPaCa2 PDAC cells in S-phase of the cell cycle within 24 hours (Fig. 6A and 6B). To determine the impact of *CPSF3* knockdown on cell cycle, we transiently knocked-down CPSF3 with siRNA in HPNE and Panc1 cells (Fig. S2D and Fig. S10G). *CPSF3* knockdown induced cell cycle arrest in Panc1 cells with minimal effect on HPNE cells (Fig. 6C and 6D). However, unlike CPSF3 inhibition-induced cell cycle arrest at S-phase, *CPSF3* knockdown cells are arrested at G2 (Fig. 6D and Fig. S12A and S12B). This pattern of cell cycle arrest is different from that induced by JTE-607 and does not resemble cell cycle arrest induced by histone defects in previous studies. This indicates that *CPSF3* knockdown-induced phenotype is indeed distinct from CPSF3 inhibition. To more specifically investigate the timing and extent of S-phase arrest upon JTE-607 treatment, we examined BrdU incorporation in a time-dependent manner (Fig. 6E). We found that JTE-607 arrests cells in early to mid S-phase of the cell cycle within 8 hours. By 24 hours, the majority of cells are arrested in S-phase. As arrest in S-phase in transformed cells can result in cell death, we assessed whether JTE-607 induces apoptosis in our PDAC cells by measuring caspase-3 and -7 activities. We found that JTE-607 did not significantly

induce apoptosis at time points where cells are mainly arrested at S-phase as compared with the positive control Doxorubicin (Fig. S13A – S13F). Overall, JTE-607 destabilizes chromatin and attenuates PDAC cell proliferation through S-phase cell cycle arrest.

DISCUSSION

Our study has several clinical implications. First, we show that *CPSF3* expression is dysregulated in PDAC and high expression correlates with poor prognosis. This is consistent with similar findings across the cancer landscape, where *CPSF3* has been reported to be a predictor of unfavorable prognosis in lung and liver cancers (Li et al. 2021; Ning et al. 2019). While several studies have experimentally manipulated various mRNA processing factors and determined the phenotypic impacts, little is known about the function of *CPSF3* in disease, particularly cancer. This is noteworthy for several reasons. First, CPSF3 is the enzymatic component of the CPA and histone mRNA processing machineries, and is thus a potentially druggable target. Second, despite acting in the same complex, knockdown of other CPA and histone mRNA processing factors can have opposing impacts on APA and histones as well as cellular phenotypes (Park et al. 2018; Zhang and Zhang 2018; Li et al. 2020; Chen et al. 2018; Fang et al. 2020; Tan et al. 2017; Pettinati et al. 2018). Recently, homozygosity in *CPSF3* missense variants was found to cause intellectual disability and embryonic lethality in humans. However, these phenotypes were completely absent in the heterozygous carriers (Arnadottir et al. 2022). In cancer cell line models, *CPSF3* is essential for cell proliferation when knocked out completely by CRISPR; however, *CPSF3* is not an essential gene upon shRNA-mediated partial knockdown (www.depmap.org). This suggests that pharmacological targeting of such an essential gene may be biologically feasible. In support of this hypothesis, we show that knockdown of *CPSF3* blocks PDAC cell proliferation and tumor growth. However, *CPSF3* knockdown does not affect cell proliferation of immortalized control cells suggesting its essentiality in highly proliferative cells. This is consistent with a recent report where sensitivity to CPSF3 inhibition is determined by high CPA activity and proliferation rate (Cui et al. 2023). Furthermore, we show that CPSF3 inhibition does not impair cell cycle progression or proliferation of immortalized control pancreatic epithelial cells, and the CPSF3 inhibitor JTE-607 is non-toxic in humans. Therefore, inhibition of CPSF3 may preferentially target transformed cells.

Recently, two groups independently demonstrated that CPSF3 is the target of the small molecule JTE-607 (Ross et al. 2020; Kakegawa et al. 2019). JTE-607 was first identified over 20 years ago as a cytokine synthesis inhibitor; however, the direct molecular target remained elusive. Despite the lack of a defined mechanism, JTE-607 was tested in a Phase I dose-escalation trial in healthy human volunteers, with no serious adverse effects (Borozdenkova et al. 2011). Therefore, despite inhibiting an essential enzyme responsible for processing pre-mRNAs, JTE-607 is not uniformly toxic in humans. This property, coupled with our data demonstrating JTE-607's anti-proliferative

effects on cancer cells, supports the contention that targeting CPSF3 is a feasible prospect in PDAC. In humans, endotoxin-induced production of C-reactive protein, IL-10 and IL-1ra was inhibited by JTE-607 (Borozdenkova et al. 2011). In animal models, JTE-607 inhibited the production of proinflammatory cytokines, prevented endotoxin shock and attenuated artificially induced lung and heart injury (Ryugo et al. 2004; Asaga et al. 2008; Kakutani et al. 1999). JTE-607 has also been used in models of acute myeloid leukemia (AML) and Ewing's sarcoma and showed growth inhibitory activity both *in vitro* and *in vivo* (xenograft models) (Tajima et al. 2010; Uesato et al. 2006; Ross et al. 2020). However, these studies were limited to leukemia and sarcoma models, with no efficacy shown for epithelial-derived tumors. Therefore, the potential for CPSF3 as a therapeutic target in adenocarcinoma was an open question. Now, we show that JTE-607 preferentially blocks proliferation of PDAC cell lines, sparing immortalized control cell lines, including epithelial cells and fibroblasts. The mechanisms underlying this difference in sensitivity are currently unknown, but may relate to variability in basal proliferation rate. We tested this hypothesis and showed that sensitivity to JTE-607 is associated with cells' proliferative state. As JTE-607 is a pro-drug that requires intracellular activation by CES1, it is possible that differences in activation of the drug between different cell lines determines strength of proliferative inhibition. However, JTE-607 sensitivity was found to be independent of CES1 expression levels (Ross et al. 2020). Finally, even though JTE-607 was first described as an inhibitor of cytokine synthesis, our RNA-seq analysis did not show an enrichment of such pathways. One possible explanation is that JTE-607 action is cell type dependent. The effects of JTE-607 in different cellular contexts and cell states warrants further investigation.

While several recent reports have linked *CPSF3* loss to defects in tumor cell growth, no study has mechanistically connected *CPSF3* to APA dysregulation. Genetic manipulation of CPA factors has been shown to alter APA patterns, dysregulate gene and protein expression and drive cancer phenotypes (Zhang et al. 2017; Fang et al. 2020; Li et al. 2021; Chen et al. 2018; Xiong et al. 2019; Brumbaugh et al. 2018; Tan et al. 2018; Chu et al. 2019; Li et al. 2020; Zhang and Zhang 2018; Park et al. 2018; Masamha et al. 2014). However, APA dynamics upon inhibition of CPSF3 activity has not been investigated. We now demonstrate that both *CPSF3* knockdown and inhibition result in APA in PDAC cells. Strikingly, CPSF3 influences APA in distinct patterns based on the mode of disruption. DAGs upon *CPSF3* knockdown and inhibition are different with only two genes commonly altered in both conditions. Additionally, we find that CPSF3 inhibition induces more lengthening events than CPSF3 knockdown. While such observation has not been reported for CPSF3, this finding is consistent with a previous study where *CLP1*, another CPA factor, mediates distinct cleavage and polyadenylation patterns when lost versus when mutated

(LaForce et al. 2022). The mechanistic differences underlying the *CPSF3* knockdown and inhibition effects raises several important questions. As CPSF3 is an integral subunit of the CPA complex, the effect of *CPSF3* knockdown and inhibition on proper recruitment of other complex components was not previously known. We demonstrated that *CPSF3* knockdown, but not inhibition, may alter the stability of CPA complex components. Importantly, however, the discrepancies between *CPSF3* knockdown and inhibition extends to the expression of CPA factors at the protein, but not mRNA level. *CPSF3* knockdown, but not inhibition, dysregulates protein expression of CPA factors. The fact that basal protein levels of CPA factors are dysregulated may explain the divergence in APA patterns and gene expression alterations. This conclusion, however, is limited to the few probed CPA complex components and further study is required for the remaining CPA complex subunits. Furthermore, whether *CPSF3* knockdown and inhibition distinctly influence PAS selection has not been previously studied. Here, we demonstrate that DAGs upon *CPSF3* knockdown and inhibition possess different motifs surrounding the PAS. Such differences have been shown to influence PAS selection thus inducing distinct APA patterns (Martin et al. 2012; Brown and Gilmartin 2003). Although *CPSF3* knockdown and inhibition affect APA differently, it remains difficult to delineate the molecular mechanism solely by computational means. It is possible that limitation of the motif algorithm may account for the differences in the enriched motifs.

JTE-607 attenuates cell proliferation in AML and Ewing's sarcoma through increasing R-loop formation and downregulating the expression of DNA damage response genes (Ross et al. 2020). R-loops are DNA:RNA hybrids that form as a result of aberrant transcription, a characteristic of cancers with genetic rearrangements such as AML and Ewing's sarcoma (Luo et al. 2022; Gorthi et al. 2018). R-loops increase in models with mRNA cleavage and polyadenylation defects (Stirling et al. 2012), suggesting that sensitivity of AML and Ewing's sarcoma to JTE-607 may be a consequence of high basal levels of R-loops, which eventually accumulate, leading to DNA damage and genomic instability. In our study, gene set enrichment analysis did not reveal changes in DNA damage response pathways upon *CPSF3* knockdown or inhibition in PDAC cells. Therefore, we propose that CPSF3 regulates cell proliferation through distinct mechanisms in AML and Ewing's sarcoma relative to PDAC. In PDAC cells, we find that JTE-607 impairs processing of proliferation-dependent (RD) histone mRNAs. This is consistent with the role of CPSF3 in the HCC (Sullivan et al. 2009b; Yang et al. 2013, 2020; Gutierrez et al. 2021; Sun et al. 2020). Defects in the HCC have been shown to reduce the availability of RD histones (Armstrong and Spencer 2021; Zhao et al. 2004; Sullivan et al. 2009a, 2009b). However, prior to now, no studies have described the effect of CPSF3 inhibition on HCC activity. Depletion of many

HCC genes led to an accumulation of histone read-through transcripts in the nucleus (Romeo et al. 2014; Wagner et al. 2007). Similarly, we find extensive transcript read-through in RD histone mRNAs, but not RI histone mRNAs upon JTE-607 treatment in PDAC cells. In accordance with a previous study, *CPSF3* knockdown did not induce RD transcriptional read-through (Pettinati et al. 2018). Importantly, neither *CPSF3* knockdown nor inhibition induced histone transcriptional read-through in immortalized control cells. This is consistent with the notion that slowly proliferating cells do not have high levels of RD histone transcription. In accordance with this model, we find that JTE-607, but not *CPSF3* knockdown, decreases mRNA levels of core histones in PDAC cells. The failure of *CPSF3* knockdown to inhibit histone gene expression may be due to the fact that a very small fraction of the total CPSF3 is present in the low abundance histone processing complex, and that complex may have a high affinity for the mCF subcomplex. On the other hand, even though it is possible that the reduction in core histone mRNA levels with JTE-607 can be attributed to defects in histone processing, a potential explanation for such reduction in histone mRNA is that the rate of cell growth has been reduced by JTE-607. Any mechanism that slows cell growth will also reduce the levels of histone mRNA. It is also possible that read-through transcription was only identified for RD histones in PDAC cells because they are abundantly transcribed. Therefore, whether this reduction of core histone mRNA levels is a direct effect of the inhibition of CPSF3 on histone mRNA processing requires further study. Additionally, although inhibition of CPSF3 will result in production of some unprocessed histone mRNA (i.e., read-through), it might also result in some polyadenylated histone mRNAs, or misprocessed histone mRNA (Lyons et al. 2016). Furthermore, it is possible that there is global transcriptional read-through upon *CPSF3* knockdown and inhibition. Knockdown of *CPSF3* results in read-through of most transcripts that are normally polyadenylated (Eaton et al. 2018, 2020). In addition, JTE-607 causes widespread transcriptional read-through in HeLa and HepG2 cells (Cui et al. 2023). However, because these read-through transcripts are very unstable, we were not able to detect them in our bulk-RNA seq data. Therefore, sequencing of nascent RNA is needed to assess the global impact on transcriptional read-through.

Several studies have shown the effect of 3'end mRNA processing on chromatin integrity. For example, JTE-607 increases accumulation in R-loops, DNA damage and thus genomic instability (Ross et al. 2020). Additionally, inhibition of CPSF4 PAS recognition upon influenza infection by the NS1 protein causes RNA Polymerase II read-through that leads to widespread changes in genome architecture dependent on NS1 (Heinz et al. 2018). We demonstrate that JTE-607 decreases core histone levels. Limited histone supplies destabilize chromatin through disruption of nucleosome assembly (Günesdogan et al. 2014). Chromatin is opened and destabilized since

cells are in S-phase replicating DNA and not producing enough histones to occupy it. We find that JTE-607 destabilizes chromatin in PDAC but not immortalized control cells, and derepresses heterochromatin-mediated gene expression silencing.

Expression of RD histones increases ~30-50 fold during DNA synthesis (Marzluff and Pandey 1988; Osley 1991). The life cycle of these core histone genes starts late in G1 through mid S phase of the cell cycle and degradation occurs at late S phase (Mendiratta et al. 2019; Marzluff et al. 2008). Silencing of the HCC core component *FLASH* induces S phase arrest in HeLa cells (Barcaroli et al. 2006). We find that JTE-607 arrests cells in the S phase of the cell cycle, with cells slowly cycling through early-mid S phase but failing to progress through late S phase. This is consistent with a previous study where depletion of the histone chaperone *ASF1* disrupts progression through mid to late S-phase (Groth et al. 2005). Importantly, silencing of *MBLAC1*, an endonuclease selective for 3' processing of RD histone pre-mRNAs, significantly impairs cell cycle progression during S-phase (Pettinati et al. 2018). In addition, knockdown of *CSTF2*, a gene with dual functions in CPA and histone pre-mRNA processing, delays progression through S phase, but its expression is highly dependent on cell cycle stage (Romeo et al. 2014). The same study showed that *CPSF3* expression is not cell cycle regulated, suggesting that the histone phenotype we observe may be driven by CPSF3 inhibition and not merely a consequence of cell cycle arrest. However, it is possible that the effect of JTE-607 on histone mRNA levels is cell cycle regulated since arrest in S-phase results in rapid degradation of histone mRNA which would quickly lower histone mRNA levels. Although *CPSF3* knockdown induced cell cycle arrest, the pattern of cell cycle arrest is distinct from that induced by JTE-607 in our study and by histone disruption in previous reports. While our manuscript was under review, a publication reported that JTE-607 leads to DNA-damage and S-phase crisis in HeLa and HepG2 cells (Cui et al. 2023). While JTE-607 induced S-phase arrest in PDAC cells, we did not see changes in DNA damage response pathways upon *CPSF3* knockdown or inhibition by gene set enrichment analysis. In fact, JTE-607 did not induce significant levels of apoptosis in our PDAC cells. Therefore, our findings suggest that JTE-607 mediates its growth attenuating phenotype by arresting cells in S-phase, possibly through reducing histone supplies thereby blocking cell cycle progression. In conclusion, our study has revealed the role of CPSF3 in pancreatic cancer and uncovered a new mechanism by which CPSF3 regulates cell proliferation.

There are several limitations to this study that warrant further investigation. First, there are clearly changes in the levels of some polyadenylated mRNAs which likely contribute to the cell proliferation deficiency, as well as some changes in alternative polyadenylation which may

544 contribute. While around 1800 genes are altered in expression, only a small number shows
545 changes in alternative polyadenylation. The contribution of CPSF3 inhibition to changes in PAS
546 selection, and the resultant effect on gene expression, require further study. Although CPSF3
547 knockdown and inhibition affect APA differently, it remains difficult to delineate the molecular
548 mechanism solely by computational means. Additionally, a main limitation in comparing CPSF3
549 knockdown and inhibition is that these approaches occur across different timescales. While we
550 address this for RD histone read-through, the different timescales may affect other observed
551 differences on the levels of gene expression and APA. While our experiments detected
552 transcriptional read-through upon JTE-607 treatment, this does not necessarily mean that those
553 transcripts are unprocessed RNAs. Rather, they fail to terminate RNA polymerase II but still they
554 could be processed, a possibility that needs further experimental investigation. Also, it is possible
555 that limitation of the motif algorithm may account for the differences in the consensus signals.
556 While our cell line models did not show APA alterations of PDAC-associated genes, we think this
557 may be attributed to the heterogeneity of PDAC tumors, and analysis of APA using patient-derived
558 single cell RNA-seq data is underway to address this issue. Although CPSF3 is an essential gene
559 in all cells including immortalized control cells, it is likely that the relatively slow growing cells upon
560 CPSF3 knockdown have adapted to grow with reduced levels of CPSF3. Furthermore, our
561 analysis provides new insight into the mechanisms underlying JTE-607 target specificity. Next, it
562 remains an open question how JTE-607 upregulates the expression of a subset of genes. It is a
563 possibility that JTE-607-induced relaxation of chromatin structure may result in aberrant
564 transcription. Similarly, even though histone mRNA transcription factors are not altered at the
565 level of APA or gene expression, open chromatin structure may facilitate transcription of
566 suppressors of histone mRNA transcription, or interaction with suppressive elements. While these
567 transcription factors bind to histone gene promoters, the fact that some of these are involved in
568 expression of many other genes must be taken into consideration. Also, it is important to keep in
569 mind that histone gene transcription requires cyclin E/cdk2 (Zhao et al. 2000), which itself is a cell
570 cycle regulator. Although the specificity of JTE-607 for CPSF3 has been supported by robust
571 experimental validation in multiple studies, it is possible that off-target effects may occur.
572 However, we note that the effects of JTE-607 on S-phase arrest and histone mRNA processing
573 are similar to those produced upon depletion of the HCC component CSTF2 (Romeo et al. 2014).

574

MATERIALS AND METHODS

Full details on all Methods are available in the Supplemental material.

Cell lines and *in vitro* culture

HEK293T, MiaPaCa2, Panc1, Suit2, Human immortalized C7 CAFs and PancPat CAFs cells were cultured in complete DMEM media. Non-transformed pancreatic cell line HPNE and HPDE cells were cultured in modified media. All cell lines were cultured at 37°C with 5% CO_2 and tested negative for Mycoplasma.

Generation of CPSF3 knockdown cells

Cells were either stably knocked-down using short-hairpin RNA (shRNA) or transiently silenced using small-interfering RNA (siRNA).

RNA isolation and quantitative PCR

Cells were lysed with TRIzol reagent. RNA was then isolated and cDNA was synthesized. qPCR was conducted with SYBR Green PCR primers mixed with iTaq Universal SYBR Green Supermix and run on CFX connect systems (Bio-Rad).

Immunoblotting

Whole cell lysates were lysed using RIPA lysis buffer with protease inhibitors, boiled at 95°C for 5min and resolved by SDS-PAGE. Proteins were transferred to nitrocellulose membranes, blocked with 5% nonfat dry milk in 1X TBST and incubated with primary antibodies overnight at 4°C. Membranes were incubated with HRP-conjugated secondary antibodies at room temperature for 1 hour and Pierce ECL Western Blotting Substrate was used for chemiluminescent detection.

Proliferation and clonogenicity assays

For proliferation experiments, cells were seeded into a white 96-well plate and cell proliferation was measured at days 0, 2, 4 and 6. For clonogenicity assays, cells were seeded into a 6-well plate and colony area was measured after 11 days.

Xenograft experiments

Animal experiments were approved by the Roswell Park Institutional Animal Care and Use Committee. MiaPaCa2 cells infected with shNTC and sh1 CPSF3 constructs were injected

subcutaneously into the flanks of 8-week old NOD/SCID/IL2Rγ$^{-/-}$ (NSG) mice. Tumor volume was determined by caliper measurements obtained in 2 dimensions and calculated as width^2 x length/2 twice a week.

Cell cycle analysis

Cells were trypsinized, fixed with 70% ethanol, washed with 1X PBS and incubated with RNaseA at 37°C for 1 hour. Propidium iodide was added and cells were analyzed by FACS at 488nm.

BrdU incorporation assay

Cells were cultured and incubated with BrdU for 4 hours, rinsed, trypsinized and permeabilized in 70% ethanol. Next, cells were pelleted and DNA was hydrolyzed in 2N HCl and then neutralized with 0.1M sodium tetraborate. Cells were pelleted and incubated with Anti-BrdU-FITC. Cell pellets were then washed and resuspended in RNaseA and PI and incubated at room temperature for 30 minutes in the dark. Cells were then analyzed by flow cytometry.

RNA-sequencing

For each condition, three biological samples were sequenced. Cell pellets were collected and sent to Roswell Park Genomic Shared Resources for RNA sequencing. Data were analyzed by the Roswell Park Bioinformatics Shared Resource.

Bioinformatics Analyses

Differential expression analyses were performed with DESeq2 (v1.36.0) (Love et al. 2014). For 3'UTR alternative polyadenylation, APA was analyzed using PolyAMiner-Bulk (Jonnakuti et al. 2023). For Motif enrichment analysis, ungapped motifs of recurring fixed-length patterns in our sequence datasets were called using the STREME methodology (Bailey et al. 2015).

Statistical analyses

Experimental findings were obtained from at least two independent experiments. $P < 0.05$ was considered statistically significant.

Data Access

All raw and processed sequencing data generated in this study will be submitted to the NCBI Gene Expression Omnibus (GEO; https://www.ncbi.nlm.nih.gov/geo/) upon final submission of the manuscript.

643

644 ## SUPPLEMENTAL MATERIAL

645 Supplemental material is available for this article.

646

647 ## ACKNOWLEDGEMENTS

648 This work was supported by National Cancer Institute (National Institutes of Health) grants P30
649 CA016056 and R25 CA181003, an award from the Roswell Park Alliance Foundation to M.E.F.,
650 and a Research Scholar Grant, RSG-21-014-01 - RMC, from the American Cancer Society M.E.F.
651 This study was also supported via funding from Prince Sattam bin Abdulaziz University project
652 number (PSAU/2023/R/1444) to A.A.A. We thank the Roswell Park Genomics and Small Molecule
653 Screening Shared Resources for their assistance. We thank Safina Alfyia for her help with the
654 MNase experiment and Brian Buckley for assistance in imaging HeLa-TI cells. We thank the
655 members of the Abel Laboratory for their insightful comments and support.

656

657

REFERENCES

Abel E V., Goto M, Magnuson B, Abraham S, Ramanathan N, Hotaling E, Alaniz AA, Kumar-Sinha C, Dziubinski ML, Urs S, et al. 2018. HNF1A is a novel oncogene that regulates human pancreatic cancer stem cell properties. *Elife* **7**: 1–35.

Armstrong C, Spencer SL. 2021. Replication-dependent histone biosynthesis is coupled to cell-cycle commitment. *Proc Natl Acad Sci U S A* **118**: 1–8.

Arnadottir GA, Oddsson A, Jensson BO, Gisladottir S, Simon MT, Arnthorsson AO, Katrinardottir H, Fridriksdottir R, Ivarsdottir E V., Jonasdottir A, et al. 2022. Population-level deficit of homozygosity unveils CPSF3 as an intellectual disability syndrome gene. *Nat Commun* **13**.

Asaga T, Ueki M, Chujo K, Taie S. 2008. JTE-607, an inflammatory cytokine synthesis inhibitor, attenuates ischemia/reperfusion-induced renal injury by reducing neutrophil activation in rats. *J Biosci Bioeng* **106**: 22–26.

Bailey P, Chang DK, Nones K, Johns AL, Patch AM, Gingras MC, Miller DK, Christ AN, Bruxner TJC, Quinn MC, et al. 2016. Genomic analyses identify molecular subtypes of pancreatic cancer. *Nature* **531**: 47–52.

Bailey TL, Johnson J, Grant CE, Noble WS. 2015. The MEME Suite. *Nucleic Acids Res* **43**: W39-49.

Barcaroli D, Bongiorno-Borbone L, Terrinoni A, Hofmann TG, Rossi M, Knight RA, Matera AG, Melino G, De Laurenzi V. 2006. FLASH is required for histone transcription and S-phase progression. *Proc Natl Acad Sci U S A* **103**: 14808–14812.

Borozdenkova S, Mant TGK, Allen E, Pu K, Hoshino S, Jurcevic S. 2011. Effects of a cytokine inhibitor, JTE-607, on the response to endotoxin in healthy human volunteers. *Int Immunopharmacol* **11**: 1837–1843. http://dx.doi.org/10.1016/j.intimp.2011.07.013.

Brown KM, Gilmartin GM. 2003. A Mechanism for the Regulation of Pre-mRNA 3′ Processing by Human Cleavage Factor Im. *Mol Cell* **12**: 1467–1476.

Brumbaugh J, Di Stefano B, Wang X, Borkent M, Forouzmand E, Clowers KJ, Ji F, Schwarz BA, Kalocsay M, Elledge SJ, et al. 2018. Nudt21 Controls Cell Fate by Connecting Alternative Polyadenylation to Chromatin Signaling. *Cell* **172**: 106-120.e21. https://doi.org/10.1016/j.cell.2017.11.023.

Cao L, Huang C, Cui Zhou D, Hu Y, Lih TM, Savage SR, Krug K, Clark DJ, Schnaubelt M, Chen L, et al. 2021. Proteogenomic characterization of pancreatic ductal adenocarcinoma. *Cell* **184**: 5031-5052.e26.

Chen X, Zhang JX, Luo JH, Wu S, Yuan GJ, Ma NF, Feng Y, Cai MY, Chen RX, Lu J, et al. 2018. CSTF2-induced shortening of the RAC1 3′UTR promotes the pathogenesis of urothelial carcinoma of the bladder. *Cancer Res* **78**: 5848–5862.

Chu Y, Elrod N, Wang C, Li L, Chen T, Routh A, Xia Z, Li W, Wagner EJ, Ji P. 2019. Nudt21 regulates the alternative polyadenylation of Pak1 and is predictive in the prognosis of

glioblastoma patients. *Oncogene* **38**: 4154–4168. http://dx.doi.org/10.1038/s41388-019-0714-9.

Collisson EA, Sadanandam A, Olson P, Gibb WJ, Truitt M, Gu S, Cooc J, Weinkle J, Kim GE, Jakkula L, et al. 2011. Subtypes of pancreatic ductal adenocarcinoma and their differing responses to therapy. *Nat Med* **17**: 500–503.

Cui Y, Wang L, Ding Q, Shin J, Cassel J, Liu Q, Salvino JM, Tian B. 2023. Elevated pre-mRNA 3' end processing activity in cancer cells renders vulnerability to inhibition of cleavage and polyadenylation. *Nat Commun* **14**: 4480.

Daily K, Patel VR, Rigor P, Xie X, Baldi P. 2011. MotifMap : integrative genome-wide maps of regulatory motif sites for model species.

Eaton JD, Davidson L, Bauer DLV, Natsume T, Kanemaki MT, West S. 2018. Xrn2 accelerates termination by RNA polymerase II, which is underpinned by CPSF73 activity. *Genes Dev* **32**: 127–139.

Eaton JD, Francis L, Davidson L, West S. 2020. A unified allosteric/torpedo mechanism for transcriptional termination on human protein-coding genes. *Genes Dev* **34**: 132–145.

Fang S, Zhang D, Weng W, Lv X, Zheng L, Chen M, Fan X, Mao J, Mao C, Ye Y, et al. 2020. CPSF7 regulates liver cancer growth and metastasis by facilitating WWP2-FL and targeting the WWP2/PTEN/AKT signaling pathway. *Biochim Biophys Acta - Mol Cell Res* **1867**.

Gorthi A, Romero JC, Loranc E, Cao L, Lawrence LA, Goodale E, Iniguez AB, Bernard X, Masamsetti VP, Roston S, et al. 2018. EWS-FLI1 increases transcription to cause R-Loops and block BRCA1 repair in Ewing sarcoma. *Nature* **555**: 387–391.

Groth A, Corpet A, Cook AJL, Roche D, Bartek J, Lukas J, Almouzni G. 2007. Regulation of replication fork progression through histone supply and demand. *Science (80-)* **318**: 1928–1931.

Groth A, Ray-Gallet D, Quivy JP, Lukas J, Bartek J, Almouzni G. 2005. Human Asf1 regulates the flow of S phase histones during replicational stress. *Mol Cell* **17**: 301–311.

Gruber AJ, Zavolan M. 2019. Alternative cleavage and polyadenylation in health and disease. *Nat Rev Genet*. http://dx.doi.org/10.1038/s41576-019-0145-z.

Günesdogan U, Jäckle H, Herzig A. 2014. Histone supply regulates S phase timing and cell cycle progression. *Elife* **3**: e02443.

Gunjan A, Paik J, Verreault A. 2005. Regulation of histone synthesis and nucleosome assembly. *Biochimie* **87**: 625–635.

Gutierrez PA, Baughman K, Sun Y, Tong L. 2021. A real-time fluorescence assay for CPSF73, the nuclease for pre-mRNA 3′-end processing. *Rna* **27**: 1148–1154.

Heinz S, Texari L, Hayes MGB, Urbanowski M, Chang MW, Givarkes N, Rialdi A, White KM, Albrecht RA, Pache L, et al. 2018. Transcription Elongation Can Affect Genome 3D Structure. *Cell* **174**: 1522-1536.e22.

Jonnakuti VS, Wagner EJ, Maletić-Savatić M, Liu Z, Yalamanchili HK. 2023. PolyAMiner-Bulk: A Machine Learning Based Bioinformatics Algorithm to Infer and Decode Alternative Polyadenylation Dynamics from bulk RNA-seq data. *bioRxiv* 2023.01.23.523471. http://biorxiv.org/content/early/2023/01/24/2023.01.23.523471.abstract.

Kakegawa J, Sakane N, Suzuki K, Yoshida T. 2019. JTE-607, a multiple cytokine production inhibitor, targets CPSF3 and inhibits pre-mRNA processing. *Biochem Biophys Res Commun* **518**: 32–37. https://doi.org/10.1016/j.bbrc.2019.08.004.

Kakutani M, Takeuchi K, Waga I, Iwamura H, Wakitani K. 1999. JTE-607, a novel inflammatory cytokine synthesis inhibitor without immunosuppression, protects from endotoxin shock in mice. *Inflamm Res* **48**: 461–468. http://link.springer.com/10.1007/s000110050487.

Kleeff J, Korc M, Apte M, La Vecchia C, Johnson CD, Biankin A V., Neale RE, Tempero M, Tuveson DA, Hruban RH, et al. 2016. Pancreatic cancer. *Nat Rev Dis Prim* **2**.

Lackford B, Yao C, Charles GM, Weng L, Zheng X, Choi EA, Xie X, Wan J, Xing Y, Freudenberg JM, et al. 2014. Fip1 regulates mRNA alternative polyadenylation to promote stem cell self-renewal. *EMBO J* **33**: 878–889.

LaForce GR, Farr JS, Liu J, Akesson C, Gumus E, Pinkard O, Miranda HC, Johnson K, Sweet TJ, Ji P, et al. 2022. Suppression of premature transcription termination leads to reduced mRNA isoform diversity and neurodegeneration. *Neuron* **110**: 1340-1357.e7. https://doi.org/10.1016/j.neuron.2022.01.018.

Li N, Jiang S, Fu R, Lv J, Yao J, Mai J, Hua X, Chen H, Liu J, Lu M. 2021. Cleavage and polyadenylation-specific factor 3 induces cell cycle arrest via PI3K/Akt/GSK-3β signaling pathways and predicts a negative prognosis in hepatocellular carcinoma. *Biomark Med* **15**: 347–358.

Li X, Ding J, Wang X, Cheng Z, Zhu Q. 2020. NUDT21 regulates circRNA cyclization and ceRNA crosstalk in hepatocellular carcinoma. *Oncogene* **39**: 891–904. http://dx.doi.org/10.1038/s41388-019-1030-0.

Liu H, Heller-Trulli D, Moore CL. 2022. Targeting the mRNA endonuclease CPSF73 inhibits breast cancer cell migration, invasion, and self-renewal. *iScience* **25**: 104804. https://doi.org/10.1016/j.isci.2022.104804.

Love MI, Huber W, Anders S. 2014. Moderated estimation of fold change and dispersion for RNA-seq data with DESeq2. *Genome Biol* **15**: 1–21.

Luo H, Zhu G, Eshelman MA, Fung TK, Lai Q, Wang F, Zeisig BB, Lesperance J, Ma X, Chen S, et al. 2022. HOTTIP-dependent R-loop formation regulates CTCF boundary activity and TAD integrity in leukemia. *Mol Cell* **82**: 833-851.e11. https://doi.org/10.1016/j.molcel.2022.01.014.

Lyons SM, Cunningham CH, Welch JD, Groh B, Guo AY, Wei B, Whitfield ML, Xiong Y, Marzluff WF. 2016. A subset of replication-dependent histone mRNAs are expressed as polyadenylated RNAs in terminally differentiated tissues. *Nucleic Acids Res* **44**: 9190–9205.

Martin G, Gruber AR, Keller W, Zavolan M. 2012. Genome-wide Analysis of Pre-mRNA 3' End Processing Reveals a Decisive Role of Human Cleavage Factor I in the Regulation of 3' UTR Length. *Cell Rep* **1**: 753–763. http://dx.doi.org/10.1016/j.celrep.2012.05.003.

Marzluff WF, Pandey NB. 1988. Multiple regulatory steps control histone mRNA concentrations. *Trends Biochem Sci* **13**: 49–52.

Marzluff WF, Wagner EJ, Duronio RJ. 2008. Metabolism and regulation of canonical histone mRNAs: Life without a poly(A) tail. *Nat Rev Genet* **9**: 843–854.

Masamha CP, Wagner EJ. 2018. The contribution of alternative polyadenylation to the cancer phenotype. *Carcinogenesis* **39**: 2–10.

Masamha CP, Xia Z, Yang J, Albrecht TR, Li M, Shyu A Bin, Li W, Wagner EJ. 2014. CFIm25 links alternative polyadenylation to glioblastoma tumour suppression. *Nature* **510**: 412–416.

Mendiratta S, Gatto A, Almouzni G. 2019. Histone supply: Multitiered regulation ensures chromatin dynamics throughout the cell cycle. *J Cell Biol* **218**: 39–54.

Moffitt RA, Marayati R, Flate EL, Volmar KE, Loeza SGH, Hoadley KA, Rashid NU, Williams LA, Eaton SC, Chung AH, et al. 2015. Virtual microdissection identifies distinct tumor- and stroma-specific subtypes of pancreatic ductal adenocarcinoma. *Nat Genet* **47**: 1168–1178.

Ning Y, Liu W, Guan X, Xie X, Zhang Y. 2019. CPSF3 is a promising prognostic biomarker and predicts recurrence of non-small cell lung cancer. *Oncol Lett* **18**: 2835–2844.

Osley MA. 1991. The regulation of histone synthesis in the cell cycle. *Annu Rev Biochem* **60**: 827–861.

Park HJ, Ji P, Kim S, Xia Z, Rodriguez B, Li L, Su J, Chen K, Masamha CP, Baillat D, et al. 2018. 3′ UTR shortening represses tumor-suppressor genes in trans by disrupting ceRNA crosstalk. *Nat Genet* **50**: 783–789.

Peng J, Sun BF, Chen CY, Zhou JY, Chen YS, Chen H, Liu L, Huang D, Jiang J, Cui GS, et al. 2019. Single-cell RNA-seq highlights intra-tumoral heterogeneity and malignant progression in pancreatic ductal adenocarcinoma. *Cell Res* **29**: 725–738. http://dx.doi.org/10.1038/s41422-019-0195-y.

Pettinati I, Grzechnik P, de Almeida CR, Brem J, McDonough MA, Dhir S, Proudfoot NJ, Schofield CJ. 2018. Biosynthesis of histone messenger RNA employs a specific 3' end endonuclease. *Elife* **7**: 1–26.

Roe J-S, Hwang C-I, Somerville TDD, Milazzo JP, Lee EJ, Da Silva B, Maiorino L, Tiriac H, Young CM, Miyabayashi K, et al. 2017. Enhancer Reprogramming Promotes Pancreatic Cancer Metastasis. *Cell* **170**: 875-888.e20. https://linkinghub.elsevier.com/retrieve/pii/S0092867417308140.

Romeo V, Griesbach E, Schümperli D. 2014. CstF64: Cell Cycle Regulation and Functional Role in 3′ End Processing of Replication-Dependent Histone mRNAs. *Mol Cell Biol* **34**: 4272–4284.

Ross NT, Lohmann F, Carbonneau S, Fazal A, Weihofen WA, Gleim S, Salcius M, Sigoillot F, Henault M, Carl SH, et al. 2020. CPSF3-dependent pre-mRNA processing as a druggable node in AML and Ewing's sarcoma. *Nat Chem Biol* **16**: 50–59.

Ryugo M, Sawa Y, Ono M, Miyamoto Y, Aleshin AN, Matsuda H. 2004. Pharmacologic preconditioning of JTE-607, a novel cytokine inhibitor, attenuates ischemia-reperfusion injury in the myocardium. *J Thorac Cardiovasc Surg* **127**: 1723–1727.

Shankar S, Pitchiaya S, Malik R, Kothari V, Hosono Y, Yocum AK, Gundlapalli H, White Y, Firestone A, Cao X, et al. 2016. KRAS Engages AGO2 to Enhance Cellular Transformation. *Cell Rep* **14**: 1448–1461. https://linkinghub.elsevier.com/retrieve/pii/S2211124716000553.

Shi Y, Manley JL. 2015. The end of the message: Multiple protein–RNA interactions define the mRNA polyadenylation site. *Genes Dev* **29**: 889–897.

Siegel RL, Miller KD, Wagle NS, Jemal A. 2023. Cancer statistics, 2023. *CA Cancer J Clin* **73**: 17–48.

Sodir NM, Kortlever RM, Barthet VJA, Campos T, Pellegrinet L, Kupczak S, Anastasiou P, Swigart LB, Soucek L, Arends MJ, et al. 2020. MYC Instructs and Maintains Pancreatic Adenocarcinoma Phenotype. *Cancer Discov* **10**: 588–607.

Stirling PC, Chan YA, Minaker SW, Aristizabal MJ, Barrett I, Sipahimalani P, Kobor MS, Hieter P. 2012. R-loop-mediated genome instability in mRNA cleavage and polyadenylation mutants. *Genes Dev* **26**: 163–175.

Sullivan KD, Mullen TE, Marzluff WF, Wagner EJ. 2009a. Knockdown of SLBP results in nuclear retention of histone mRNA. *Rna* **15**: 459–472.

Sullivan KD, Steiniger M, Marzluff WF. 2009b. A Core Complex of CPSF73, CPSF100, and Symplekin May Form Two Different Cleavage Factors for Processing of Poly(A) and Histone mRNAs. *Mol Cell* **34**: 322–332. http://dx.doi.org/10.1016/j.molcel.2009.04.024.

Sun Y, Zhang Y, Aik WS, Yang XC, Marzluff WF, Walz T, Dominski Z, Tong L. 2020. Structure of an active human histone pre-mRNA 3′-end processing machinery. *Science (80-)* **367**: 700–703.

Tajima N, Fukui K, Uesato N, Maruhashi J, Yoshida T, Watanabe Y, Tojo A. 2010. JTE-607, a multiple cytokine production inhibitor, induces apoptosis accompanied by an increase in p21waf1/cip1 in acute myelogenous leukemia cells. *Cancer Sci* **101**: 774–781.

Tan S, Ding K, Chong QY, Zhao J, Liu Y, Shao Y, Zhang Y, Yu Q, Xiong Z, Zhang W, et al. 2017. Post-transcriptional regulation of ERBB2 by miR26a/b and HuR confers resistance to tamoxifen in estrogen receptor-positive breast cancer cells. *J Biol Chem* **292**: 13551–13564.

Tan S, Li H, Zhang W, Shao Y, Liu Y, Guan H, Wu J, Kang Y, Zhao J, Yu Q, et al. 2018. NUDT21 negatively regulates PSMB2 and CXXC5 by alternative polyadenylation and contributes to hepatocellular carcinoma suppression. *Oncogene* **37**: 4887–4900. http://dx.doi.org/10.1038/s41388-018-0280-6.

Uesato N, Fukui K, Maruhashi J, Tojo A, Tajima N. 2006. JTE-607, a multiple cytokine production inhibitor, ameliorates disease in a SCID mouse xenograft acute myeloid leukemia model. *Exp Hematol* **34**: 1385–1392.

Venkat S, Alahmari AA, Feigin ME. 2021. Drivers of Gene Expression Dysregulation in Pancreatic Cancer. *Trends in Cancer* **7**: 594–605. https://doi.org/10.1016/j.trecan.2021.01.008.

Venkat S, Tisdale AA, Schwarz JR, Alahmari AA, Maurer HC, Olive KP, Eng KH, Feigin ME. 2020. Alternative polyadenylation drives oncogenic gene expression in pancreatic ductal adenocarcinoma. *Genome Res* 1–14.

Wagner EJ, Burch BD, Godfrey AC, Salzler HR, Duronio RJ, Marzluff WF. 2007. A Genome-wide RNA Interference Screen Reveals that Variant Histones Are Necessary for Replication-Dependent Histone Pre-mRNA Processing. *Mol Cell* **28**: 692–699.

Wang L, Yang H, Zamperone A, Diolaiti D, Palmbos PL, Abel E V., Purohit V, Dolgalev I, Rhim AD, Ljungman M, et al. 2019. ATDC is required for the initiation of KRAS-induced pancreatic tumorigenesis. *Genes Dev* **33**: 641–655. http://genesdev.cshlp.org/lookup/doi/10.1101/gad.323303.118.

Xiao L, Somers K, Murray J, Pandher R, Karsa M, Ronca E, Bongers A, Terry R, Ehteda A, Gamble LD, et al. 2021. Dual targeting of chromatin stability by the curaxin CBL0137 and histone deacetylase inhibitor panobinostat shows significant preclinical efficacy in neuroblastoma. *Clin Cancer Res* **27**: 4338–4352.

Xiong M, Chen L, Zhou L, Ding Y, Kazobinka G, Chen Z, Hou T. 2019. NUDT21 promotes bladder cancer progression through ANXA2 and LIMK2 by alternative polyadenylation. *Theranostics* **9**: 7156–7167.

Yalamanchili HK, Alcott CE, Ji P, Wagner EJ, Zoghbi HY, Liu Z. 2020. PolyA-miner: Accurate assessment of differential alternative poly-adenylation from 3′Seq data using vector projections and non-negative matrix factorization. *Nucleic Acids Res* **48**: 1–12.

Yang X-C, Sabath I, Debski J, Kaus-Drobek M, Dadlez M, Marzluff WF, Dominski Z. 2013. A Complex Containing the CPSF73 Endonuclease and Other Polyadenylation Factors Associates with U7 snRNP and Is Recruited to Histone Pre-mRNA for 3'-End Processing. *Mol Cell Biol* **33**: 28–37.

Yang X, Sun Y, Aik WS, Marzluff WF, Tong L, Dominski Z. 2020. Studies with recombinant U7 snRNP demonstrate that CPSF73 is both an endonuclease and a 5'-3' exonuclease. *Rna* rna.076273.120.

Yuan F, Hankey W, Wagner EJ, Li W, Wang Q. 2019. Alternative polyadenylation of mRNA and its role in cancer. *Genes Dis*.

Zhang B, Liu Y, Liu D, Yang L. 2017. Targeting cleavage and polyadenylation specific factor 1 via shRNA inhibits cell proliferation in human ovarian cancer. *J Biosci* **42**: 417–425.

Zhang L, Zhang W. 2018. Knockdown of NUDT21 inhibits proliferation and promotes apoptosis of human K562 leukemia cells through ERK pathway. *Cancer Manag Res* **10**: 4311–4323.

888 Zhao J, Kennedy BK, Lawrence BD, Barbie DA, Gregory Matera A, Fletcher JA, Harlow E.
889 2000. NPAT links cyclin E-Cdk2 to the regulation of replication-dependent histone gene
890 transcription. *Genes Dev* **14**: 2283–2297.

891 Zhao X, McKillop-Smith S, Müller B. 2004. The human histone gene expression regulator
892 HBP/SLBP is required for histone and DNA synthesis, cell cycle progression and cell
893 proliferation in mitotic cells. *J Cell Sci* **117**: 6043–6051.

894

Figure Legends

FIGURE 1. *CPSF3* is highly expressed in PDAC and is required for PDAC cell proliferation. **(A)** *CPSF3* mRNA expression from CPTAC PDAC patient data. Whiskers indicate minimum and maximum data points. ***, *P*<0.0001, Ordinary one-way ANOVA with Tukey multiple comparisons test. **(B)** *CPSF3* mRNA expression from PDAC patient data (TCGA) as compared to normal pancreas (GTEx). Whiskers indicate minimum and maximum data points. ***, *P*<0.0001, unpaired t test with Welch's correction. **(C)** Immunoblot of CPSF3 in immortalized control pancreatic epithelial cells (black) and PDAC cells (red). **(D)** Kaplan Meier survival curves of PDAC patients with high (red) and low (blue) *CPSF3* mRNA levels. Data were obtained from CPTAC database. **(E)** Immunoblot of CPSF3 in shNTC, sh1 and sh2 CPSF3 knockdown cells. **(F)** Proliferation rates at days 0, 2, 4 and 6 of shNTC (blue), sh1 (orange) and sh2 (green) CPSF3 knockdown cells. **, $P < 0.01$; ***, $P < 0.001$; 2-way ANOVA with Dunnett's multiple comparisons test. **(G)** Mean Tumor Volume (mm^3) of CPSF3-knockdown (orange) and control (blue) MiaPaCa2 tumors. ***, $P < 0.001$, 2-way ANOVA.

FIGURE 2. PDAC cell lines are sensitive to CPSF3 inhibition by JTE-607. **(A)** IC50 of JTE-607 on immortalized control (HPNE and HPDE) and PDAC (MiaPaCa2, Panc1, Suit2, BxPC3) cell lines after 72 hr of treatment. **(B)** IC50 of JTE-607 on human fibroblast C7 and PancPat CAFs after 72 hr of treatment. **(C)** Association between doubling time and IC50 of JTE-607 in pancreatic cell lines. Red denotes PDAC cells while Black denotes immortalized control cell lines. $R^2 = 0.4995$. **(D, E)** Proliferation rates at days 0, 2, 4 and 6 of immortalized control and PDAC cell lines after treatment with escalating concentrations of JTE-607. *, $P < 0.05$; 2-way ANOVA with Dunnett's multiple comparisons test. Data are shown as mean ± SEM. **(F)** Clonogenic growth assay of PDAC cell lines after treatment with increasing concentration of JTE-607.

FIGURE 3. JTE-607 decreases gene expression of replication-dependent histones. **(A)** Heatmap of top differentially expressed genes after 24 hr of 10μM JTE-607 treatment. Replication-dependent histones are colored in blue. Expression is plotted as transformed expression value. **(B)** DSeq2 normalized counts of *H3F3A* and *H2AZ1* histone variants (replication-independent) in Panc1 cells treated with 10μM JTE-607 for 24 hr. **, P < 0.001. **(C)** mRNA expression of *H2B (HIST1H2BC)* and *H3 (HIST1H3B)* in MiaPaCa2 cells treated with JTE-607. *, $P < 0.05$, **, $P < 0.01$, ***, $P < 0.001$, Ordinary one-way ANOVA with Dunnett's multiple comparisons test. **(D, E)** Survival analyses of low (blue) and high (red) expression of the RD histone signature (50 genes) in the TCGA-PAAD dataset. Signature genes were uploaded to GEPIA2 to assess disease-free **(D)** and overall survival **(E)** based on median.

FIGURE 4. JTE-607 induces replication-dependent histone transcriptional read-through. **(A, B)** Quantification of replication-dependent histone read-through in Panc1 and HPNE cells after 24 hr **(A)** and 2 hr **(B)** of 10μM JTE-607 treatment by RT-qPCR. Data were normalized to DMSO controls (Dashed horizontal line). *, $P < 0.05$; **, $P < 0.01$; ***, $P < 0.001$; 2-way ANOVA with Sidak's multiple comparisons test. **(C, D)** Quantification of replication-independent histone read-through in Panc1 and HPNE cells after 24 hr **(C)** and 2 hr **(D)** of 10μM JTE-607 treatment by RT-qPCR. Data were normalized to DMSO controls (Dashed horizontal line). *, $P < 0.05$; **, $P < 0.01$; ***, $P < 0.001$; 2-way ANOVA with Sidak's multiple comparisons test.

FIGURE 5. JTE-607 induces chromatin instability selectively in PDAC cells. **(A)** Micrococcal Nuclease assay of Panc1 cells treated with 10μM JTE-607 or 1μM CBL0137. **(B)** Micrococcal Nuclease assay of immortalized HPNE control cells treated with the CPSF3 inhibitor JTE-607 (10μM) or CBL0137 (1μM). **(C)** GFP+ HeLa-TI cells following 10μM JTE-607 or 1μM

CBL0137 treatment. **(D)** Fold change of GFP+ HeLa-TI from **(C).** ***, $P < 0.0001$; 2-way ANOVA with Tukey's multiple comparisons test. **(E)** Flow cytometry analysis of GFP+ HeLa-TI cells following 10μM JTE-607 or 1μM CBL0137 treatment. Fold change is shown as mean ± SEM of two independent experiments. **, $P < 0.01$, ***, $P < 0.0001$, Ordinary one-way ANOVA with Tukey's multiple comparisons test.

FIGURE 6. JTE-607 impairs cell cycle progression by inducing S-phase arrest.
(A, B) Cell cycle distribution and quantification of HPNE, MiaPaCa2 and Panc1 cell lines treated with 1-10μM JTE-607. *, $P < 0.05$, **, $P < 0.001$, ***, $P < 0.0001$, 2-way ANOVA with Dunnett's multiple comparisons test. **(C, D)** Cell cycle distribution and quantification of HPNE and Panc1 cell lines upon transient *CPSF3* knockdown by siRNA after 24 hr of transfection. siCTL = non-targeting control siRNA. *, $P < 0.01$, **, $P < 0.001$, 2-way ANOVA with Dunnett's multiple comparisons test. Quantification in panels **(B)** and **(D)** are the number of cells in S-phase**. (E)** BrdU incorporation assay showing cell cycle population upon JTE-607 treatment. Lower left quadrant represents G1 population. Lower right quadrant represents G2 population. The top two quadrants represent S phase populations; early S-phase (left) and late S-phase (right).

Figure 1

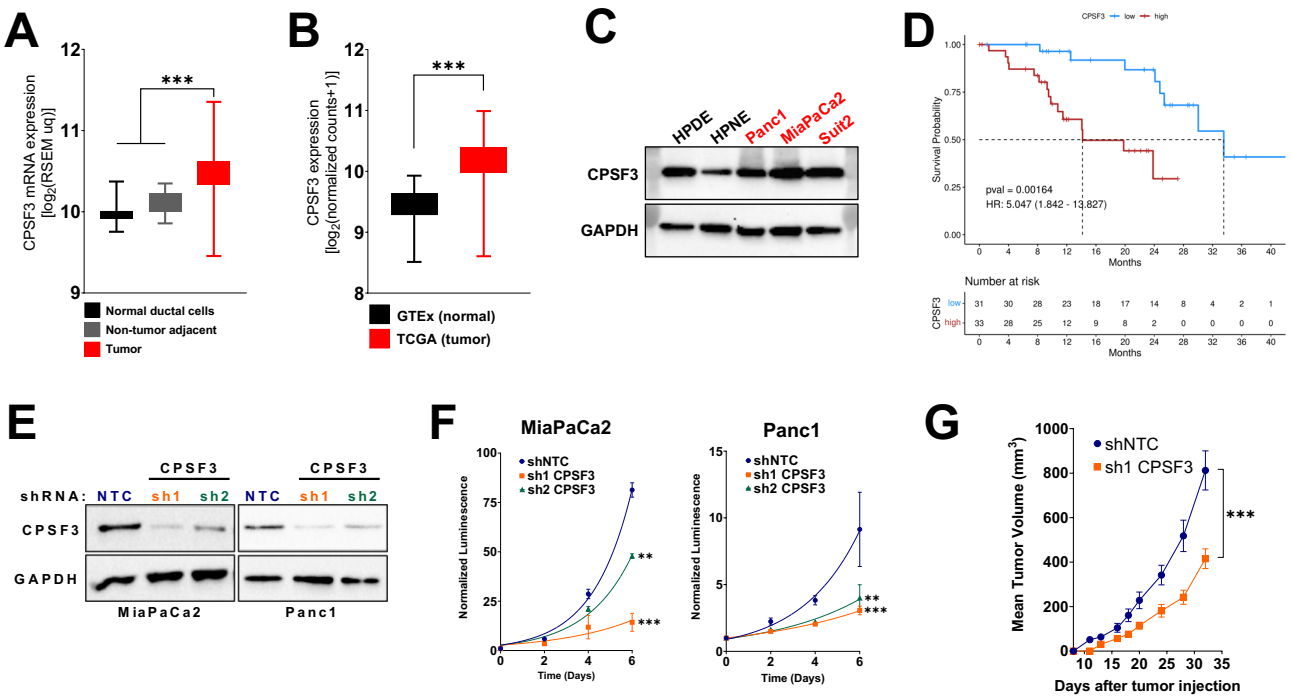
A
CPSF3 mRNA expression [log2(RSEM uq)]
***
Normal ductal cells
Non-tumor adjacent
Tumor
B
CPSF3 expression [log2(normalized counts+1)]
***
GTEx (normal)
TCGA (tumor)
C
HPDE
HPNE
Panc1
MiaPaCa2
Suit2
CPSF3
GAPDH
D
CPSF3 low high
Survival Probability
pval = 0.00164
HR: 5.047 (1.842 - 13.827)
Months
Number at risk
CPSF3 low 31 30 28 23 18 17 14 8 4 2 1
high 33 28 25 12 9 8 2 0 0 0 0
Months
E
CPSF3
CPSF3
shRNA: NTC sh1 sh2 NTC sh1 sh2
CPSF3
GAPDH
MiaPaCa2
Panc1
F
MiaPaCa2
Panc1
shNTC
sh1 CPSF3
sh2 CPSF3
Normalized Luminescence
Time (Days)
**
***
G
shNTC
sh1 CPSF3
Mean Tumor Volume (mm3)
***
Days after tumor injection

Figure 2

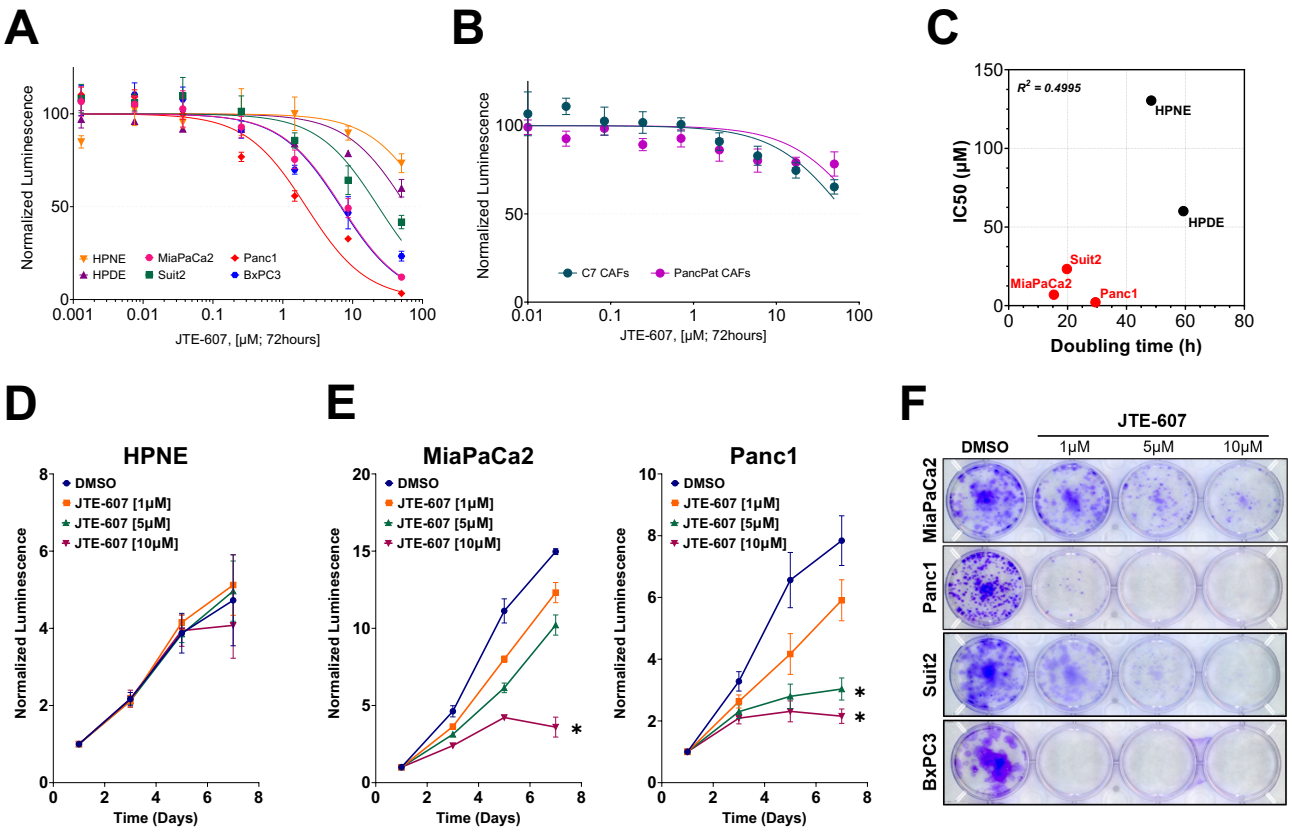
A
Normalized Luminescence
JTE-607, [μM; 72hours]
HPNE
HPDE
MiaPaCa2
Suit2
Panc1
BxPC3
B
Normalized Luminescence
JTE-607, [μM; 72hours]
C7 CAFs
PancPat CAFs
C
IC50 (μM)
Doubling time (h)
R² = 0.4995
HPNE
HPDE
Suit2
MiaPaCa2
Panc1
D
HPNE
Normalized Luminescence
Time (Days)
DMSO
JTE-607 [1μM]
JTE-607 [5μM]
JTE-607 [10μM]
E
MiaPaCa2
Panc1
Normalized Luminescence
Time (Days)
DMSO
JTE-607 [1μM]
JTE-607 [5μM]
JTE-607 [10μM]
*
F
JTE-607
DMSO
1μM
5μM
10μM
MiaPaCa2
Panc1
Suit2
BxPC3

Figure 3

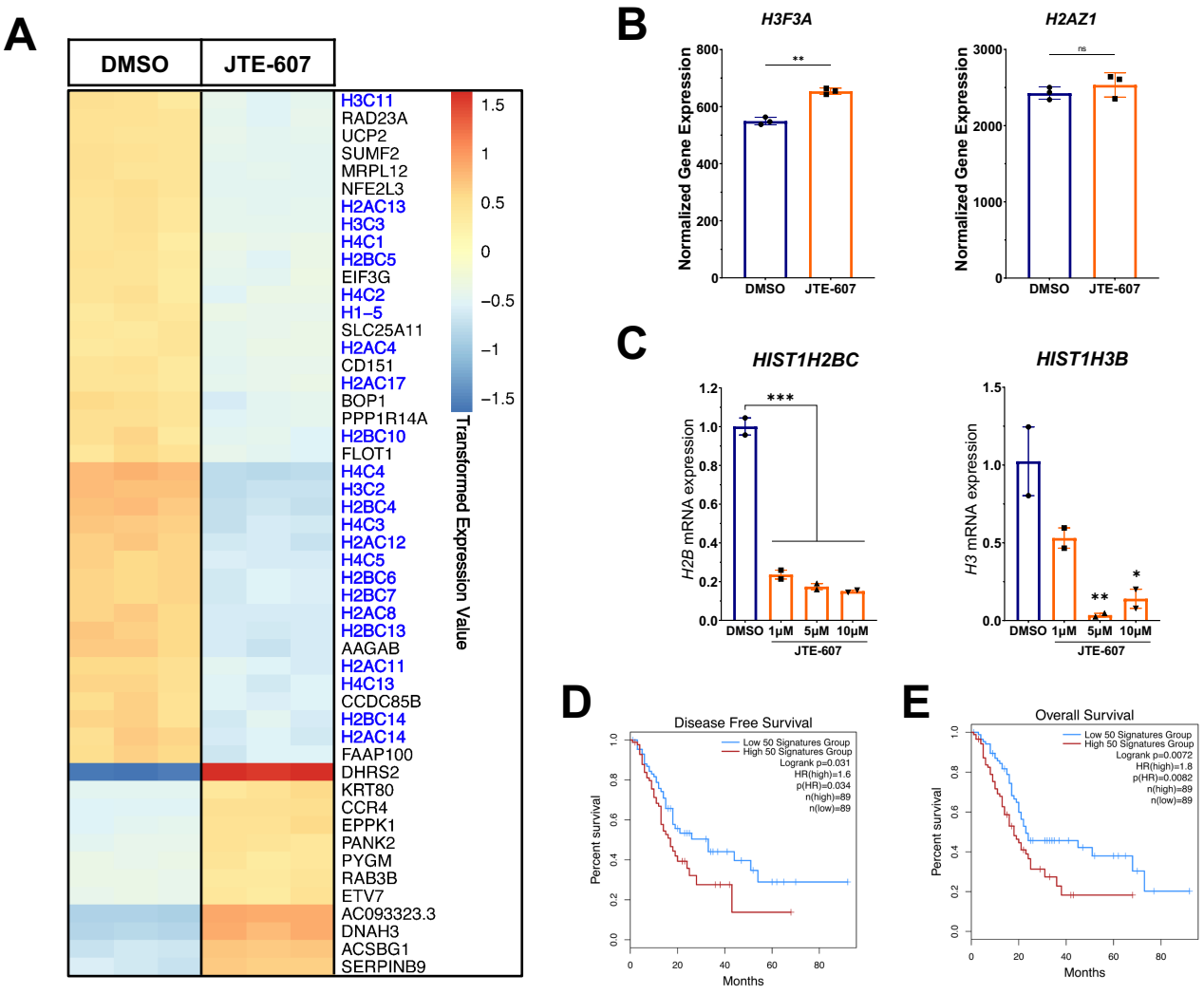
A
DMSO
JTE-607
H3C11
RAD23A
UCP2
SUMF2
MRPL12
NFE2L3
H2AC13
H3C3
H4C1
H2BC5
EIF3G
H4C2
H1–5
SLC25A11
H2AC4
CD151
H2AC17
BOP1
PPP1R14A
H2BC10
FLOT1
H4C4
H3C2
H2BC4
H4C3
H2AC12
H4C5
H2BC6
H2BC7
H2AC8
H2BC13
AAGAB
H2AC11
H4C13
CCDC85B
H2BC14
H2AC14
FAAP100
DHRS2
KRT80
CCR4
EPPK1
PANK2
PYGM
RAB3B
ETV7
AC093323.3
DNAH3
ACSBG1
SERPINB9
1.5
1
0.5
0
−0.5
−1
−1.5
Transformed Expression Value
B
H3F3A
H2AZ1
Normalized Gene Expression
DMSO
JTE-607
**
ns
C
HIST1H2BC
HIST1H3B
H2B mRNA expression
H3 mRNA expression
***
DMSO 1μM 5μM 10μM
JTE-607
D
Disease Free Survival
Low 50 Signatures Group
High 50 Signatures Group
Logrank p=0.031
HR(high)=1.6
p(HR)=0.034
n(high)=89
n(low)=89
Percent survival
Months
E
Overall Survival
Low 50 Signatures Group
High 50 Signatures Group
Logrank p=0.0072
HR(high)=1.8
p(HR)=0.0082
n(high)=89
n(low)=89
Percent survival
Months

Figure 4

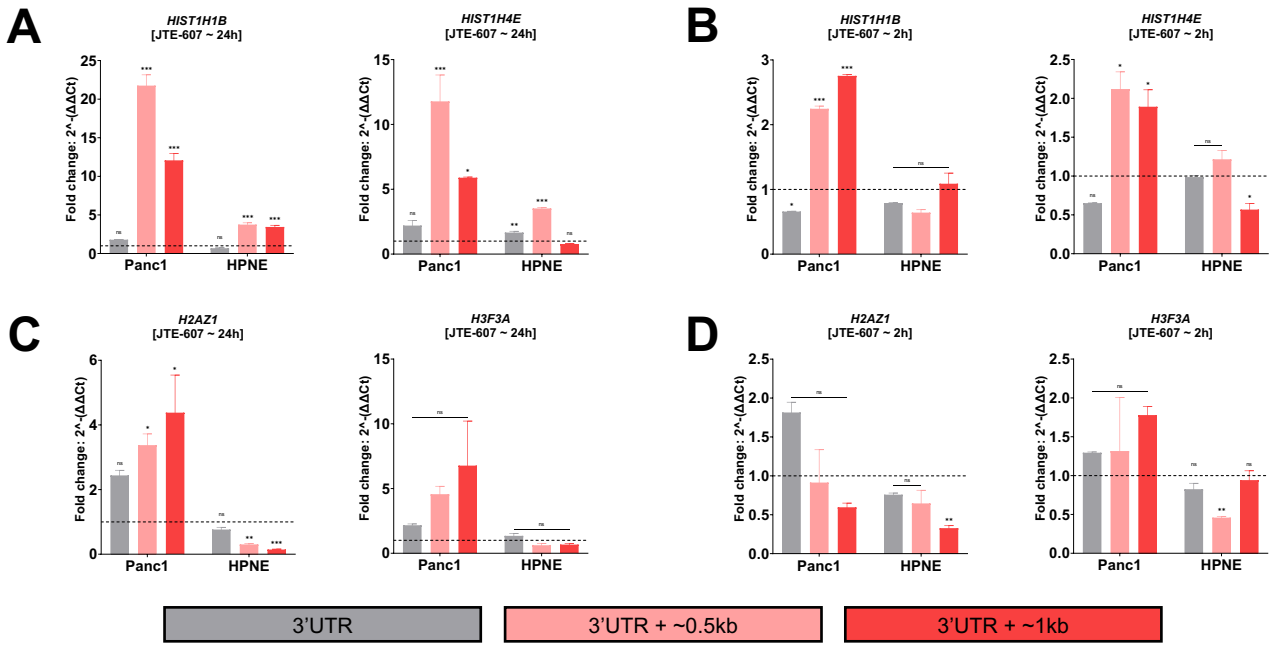
A
HIST1H1B
[JTE-607 ~ 24h]
HIST1H4E
[JTE-607 ~ 24h]
B
HIST1H1B
[JTE-607 ~ 2h]
HIST1H4E
[JTE-607 ~ 2h]
C
H2AZ1
[JTE-607 ~ 24h]
H3F3A
[JTE-607 ~ 24h]
D
H2AZ1
[JTE-607 ~ 2h]
H3F3A
[JTE-607 ~ 2h]
Fold change: 2^-(ΔΔCt)
Panc1
HPNE
3'UTR
3'UTR + ~0.5kb
3'UTR + ~1kb

Figure 5

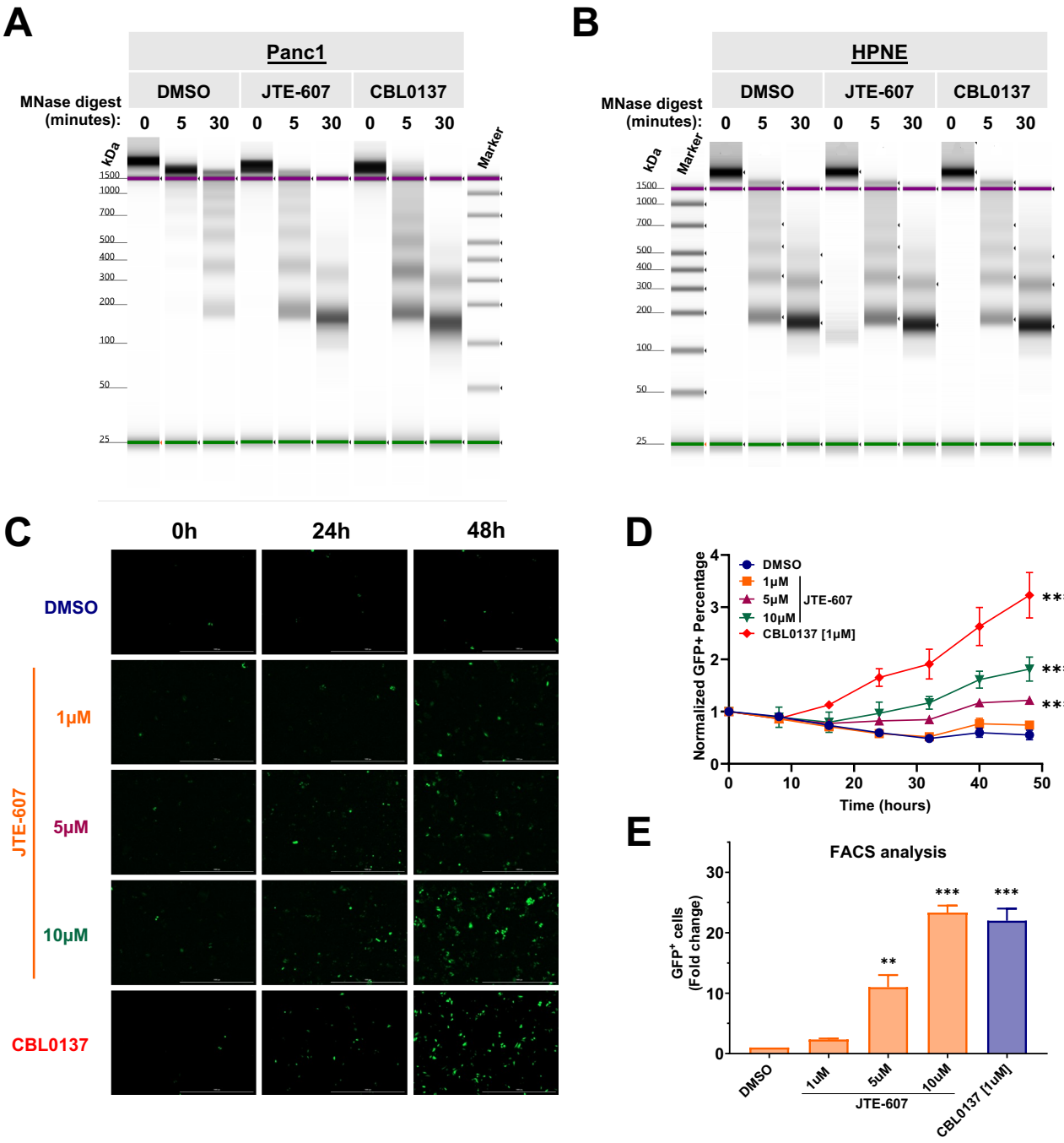
A
Panc1
DMSO
JTE-607
CBL0137
MNase digest (minutes):
0 5 30 0 5 30 0 5 30
kDa
Marker
1500
1000
700
500
400
300
200
100
50
25
B
HPNE
DMSO
JTE-607
CBL0137
MNase digest (minutes):
0 5 30 0 5 30 0 5 30
kDa
Marker
1500
1000
700
500
400
300
200
100
50
25
C
0h
24h
48h
DMSO
1μM
5μM
10μM
JTE-607
CBL0137
D
DMSO
1μM
5μM
10μM
JTE-607
CBL0137 [1μM]
Normalized GFP+ Percentage
Time (hours)
0
10
20
30
40
50
1
2
3
4
***
***
***
E
FACS analysis
GFP+ cells (Fold change)
0
10
20
30
**
***
***
DMSO
1uM
5uM
10uM
JTE-607
CBL0137 [1uM]

Figure 6

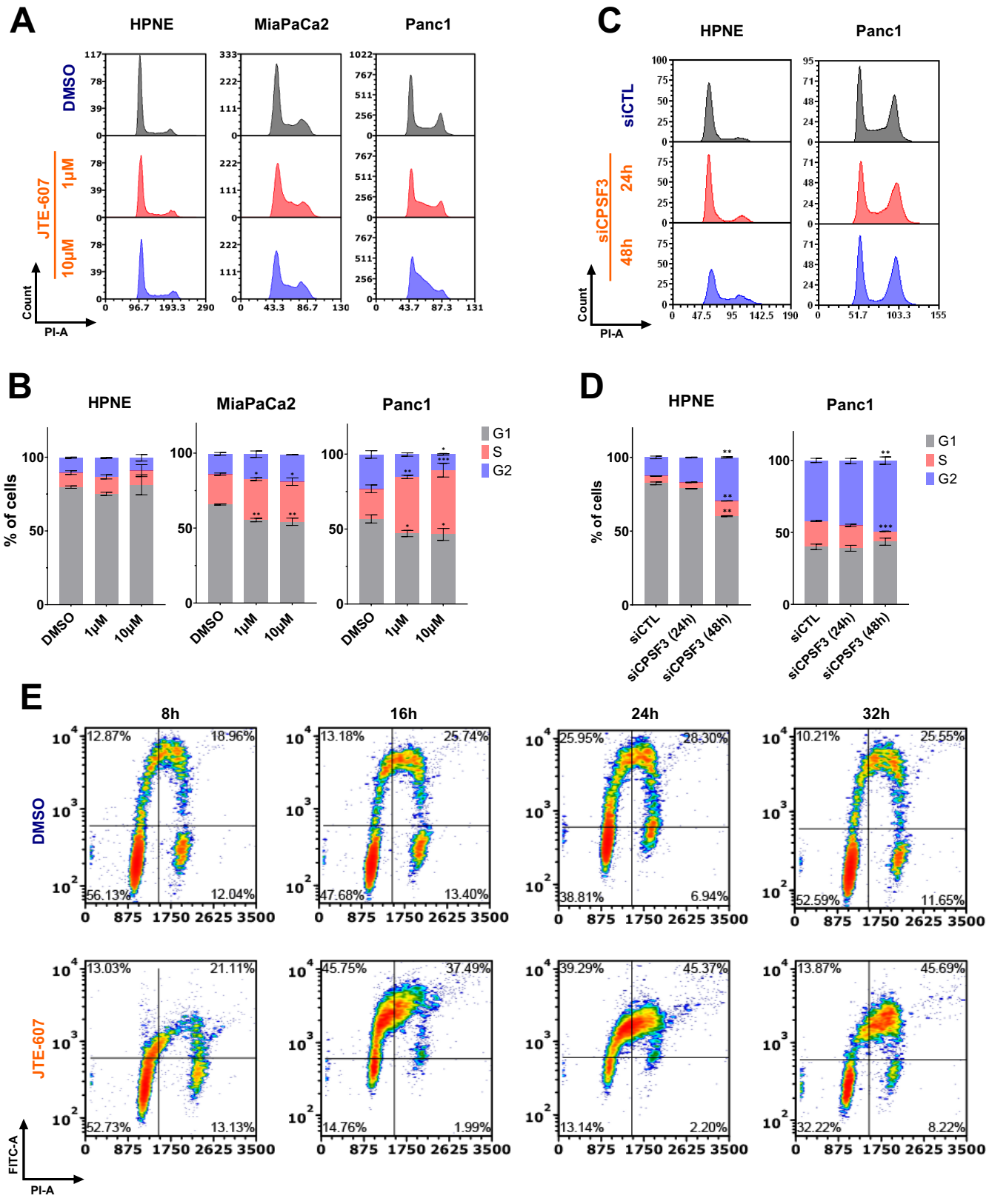
A
HPNE
MiaPaCa2
Panc1
DMSO
JTE-607
1μM
10μM
Count
PI-A
C
HPNE
Panc1
siCTL
siCPSF3
24h
48h
Count
PI-A
B
HPNE
MiaPaCa2
Panc1
% of cells
G1
S
G2
DMSO
1μM
10μM
D
HPNE
Panc1
% of cells
G1
S
G2
siCTL
siCPSF3 (24h)
siCPSF3 (48h)
E
8h
16h
24h
32h
DMSO
JTE-607
12.87%
18.96%
56.13%
12.04%
13.18%
25.74%
47.68%
13.40%
25.95%
28.30%
38.81%
6.94%
10.21%
25.55%
52.59%
11.65%
13.03%
21.11%
52.73%
13.13%
45.75%
37.49%
14.76%
1.99%
39.29%
45.37%
13.14%
2.20%
13.87%
45.69%
32.22%
8.22%
FITC-A
PI-A

CPSF3 inhibition blocks pancreatic cancer cell proliferation through disruption of core histone mRNA processing

Abdulrahman A Alahmari, Aditi H Chaubey, Venkata S Jonnakuti, et al.

RNA published online January 8, 2024